Journal of Pharmacological Sciences 127 (2015) 145–149

Contents lists available at ScienceDirect

Journal of Pharmacological Sciences

journal homepage: www.elsevier.com/locate/jphs

Short communication

Paroxetine prevented the down-regulation of astrocytic L-Glu transporters in neuroinflammation

Koki Fujimori [a, b], Junpei Takaki [a, b], Yukari Shigemoto-Mogami [a], Yuko Sekino [a], Takeshi Suzuki [b], Kaoru Sato [a, *]

[a] Laboratory of Neuropharmacology, Division of Pharmacology, National Institute of Health Sciences, 1-18-1 Kamiyoga, Setagaya-ku, Tokyo 158-8501, Japan
[b] Division of Basic Biological Science, Faculty of Pharmacy, Keio University, 1-5-30 Shiba-koen, Minato-ku, Tokyo 105-8512, Japan

ARTICLE INFO

Article history:
Received 4 August 2014
Received in revised form
26 August 2014
Accepted 18 September 2014
Available online 2 October 2014

Keywords:
Paroxetine
L-glutamate
Inflammation

ABSTRACT

The extracellular L-glutamate (L-Glu) concentration is elevated in neuroinflammation, thereby causing excitotoxicity. One of the mechanisms is down-regulation of astrocyte L-Glu transporters. Some antidepressants have anti-inflammatory effects. We therefore investigated effects of various antidepressants on the down-regulation of astrocyte L-Glu transporters in the in vitro neuroinflammation model. Among these antidepressants, only paroxetine was effective. We previously demonstrated that the down-regulation of astrocyte L-Glu transporters was caused by L-Glu released from activated microglia. We here clarified that only paroxetine inhibited L-Glu release from microglia. This is the novel action of paroxetine, which may bring advantages on the therapy of neuroinflammation.

Increasing evidence indicates that inflammatory processes play important roles in the pathogenesis of many neurodegenerative disorders (1–3). Under the neuroinflammatory conditions, it is known that the extracellular concentration of L-glutamate (L-Glu) and inflammatory mediators, such as proinflammatory cytokines, prostaglandins, free radicals and complements are elevated (4). L-Glu is one of the most abundant excitatory neurotransmitters in the mammalian CNS. The released L-Glu is immediately uptaken by astrocyte L-Glu transporters, GLAST (EAAT1 in human) and GLT-1 (EAAT2 in human), or sustained elevation of extracellular concentration of L-Glu induce excitotoxicity. The impairment of the astrocyte L-Glu transporters is reported in various neurological disorders including Alzheimer's disease (5), Parkinson's diseases (6) and amyotrophic lateral sclerosis (7). We found that the expression level of L-Glu transporters in astrocytes of astrocyte-microglia-neuron mixed culture was decreased in the *in vitro* model of the early stage of inflammation in the previous study (8). We clarified the interaction between astrocytes and microglia underlie the down-regulation of L-Glu transporters, i.e., activated microglia release L-Glu and the resulting elevation of extracellular L-Glu cause down-regulation of astrocytic L-Glu transporters. Some antidepressants are known to have anti-inflammatory effects (9, 10). In this study, therefore, we investigated the effects of various antidepressants on the decrease in the astrocytic L-Glu transporter function in the early stage of inflammation and the contribution of microglia to the effects.

Astrocyte-microglia-neuron mixed culture and microglia culture were performed according to the methods previously described (8). Antidepressants and serotonin (5-HT) were dissolved in PBS at 100 μM and 10 mM, respectively, and were diluted with culture medium at the time of use. At 8 DIV, the astrocyte-microglia-neuron mixed culture was treated with 10 ng/mL LPS for 72 h. Antidepressants were applied from 1 h before to the end of the LPS-treatment. Then the concentration of the L-Glu remaining in the culture medium 30 min after changing extracellular concentration of L-Glu to 100 μM was measured. The measurement of the extracellular L-Glu concentration in the medium was performed according to the methods previously described (8). Real-Time Quantitative RT-PCR, Western blotting, immunocytochemistry were also performed according to the methods previously

Abbreviations: ATP, adenosine 5′-triphosphate; CNS, central nervous system; DIV, days *in vitro*; GABA, γ-aminobutyric acid; L-glu, L-glutamate; LPS, lipopolysaccharide; PBS, phosphate-buffered saline; $P2X_4$, P2X prinoceptor 4; RNA, ribonucleic acid; SD, Sprague-Dawley; SDS, sodium dodecyl sulfate; SNRI, serotonin–norepinephrine reuptake inhibitor; SSRI, selective serotonin reuptake inhibitor; TCA, tricyclic antidepressant; 5-HT, 5-hydroxytryptamine.

* Corresponding author. Tel./fax: +81 3 3700 9698.
E-mail address: kasato@nihs.go.jp (K. Sato).

Peer review under responsibility of Japanese Pharmacological Society.

http://dx.doi.org/10.1016/j.jphs.2014.09.002

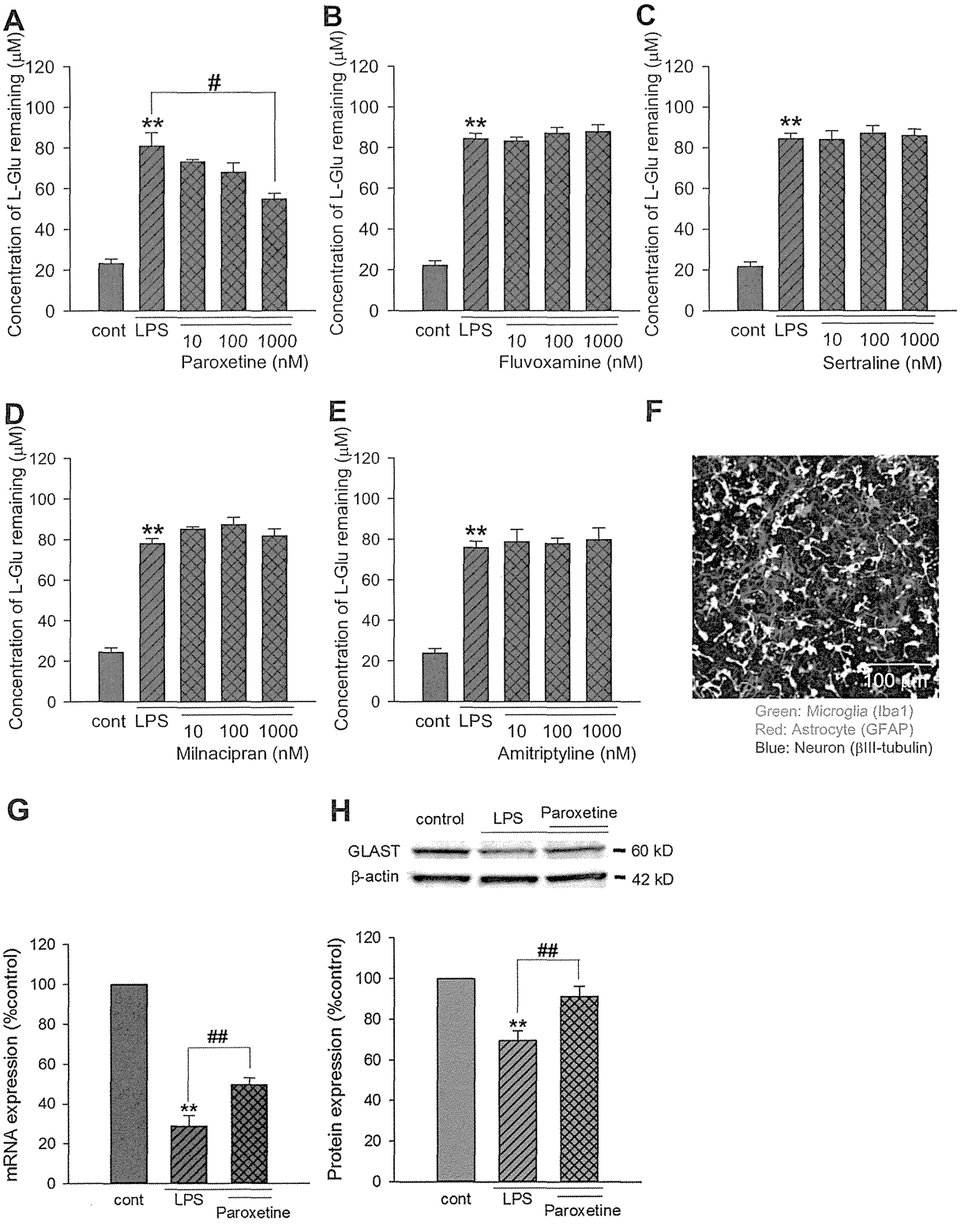

Fig. 1. Effects of antidepressants on the decreased L-Glu transport activity under the inflammatory condition. A–E. Antidepressants were applied to the mixed culture from 1 h before to the end of the LPS-treatment (10 ng/ml, 72 h). L-Glu transport activity was quantified as the L-Glu remaining 30 min after changing the extracellular concentration to 100 μM. Paroxetine prevented the LPS-induced decrease in the L-Glu transport activity in a concentration-dependent manner (A). Fluvoxamine (B), sertraline (C), milnacipran (D), and amitriptyline (E) had no effects. **: $p < 0.01$ vs. control group, #: $p < 0.05$ vs. LPS-treated group, Tukey's test following ANOVA ($N = 6$). F. Typical image of the microglia-astrocyte-neuron mixed culture immunostained with cell type-specific markers (Iba1: microglia; GFAP: astrocytes; βIII tubulin: neurons). G, H. Effects of paroxetine on the expression level of GLAST. Mixed cultures were treated with LPS (10 ng/ml) in the absence or presence of the paroxetine for 24 h (for mRNA level quantification) or 72 h (for protein level quantification). The expression level of GLAST was quantified at mRNA level (G) and protein level (H). LPS (10 ng/ml) caused significant decrease in GLAST mRNA level and paroxetine significantly prevented the decrease (G). LPS (10 ng/ml) caused significant decrease in GLAST protein level and paroxetine almost completely prevented the decrease (H). **: $p < 0.01$ vs. control group, ##: $p < 0.01$ vs. LPS-treated group, Tukey's test following ANOVA ($N = 5$).

described (8). The microglia culture was treated with LPS for 24 h in the presence or absence of antidepressants and the concentration of L-Glu in the medium was measured. All sets of the experiments were repeated in triplicate. All procedures described above were in accordance with institutional guidelines.

In the previous report, we showed that the expression level of astrocytic L-Glu transporters was decreased in the astrocyte-microglia-neuron mixed culture in LPS (10 ng/ml, 72 h)-induced inflammation model without cell death (8). We first compared the effects of various groups of antidepressants, i.e., selective serotonin reuptake inhibitors (SSRIs) (paroxetine, fluvoxamine, and sertraline), serotonin–norepinephrine reuptake inhibitor (SNRI) (milnacipran), and tricyclic antidepressant (TCA) (amitriptyline), on the decrease in the astrocytic L-Glu transporter function in this inflammation model. To quantify L-Glu transport activity, we measured the concentration of L-Glu remaining 30 min after changing the medium to the one containing 100 μM of L-Glu. In each set of experiment, LPS-induced decrease in the L-Glu transport activity was stably reproduced (Fig. 1A–E). Among antidepressants, only paroxetine prevented the LPS-induced decrease in L-Glu transport activity (Fig. 1A). The effect was concentration-dependent and reached significant at 1 μM. The other antidepressants had no effects (Fig. 1B–E). Typical image of the astrocyte-microglia-neuron mixed culture was shown in Fig. 1F. We have clarified that LPS-induced decrease in L-Glu transport activity was caused by the decrease in the expression level of GLAST, a predominant L-Glu transporter in the mixed culture, in both of mRNA and protein levels (8). In this study, LPS-induced decreases in the expression of GLAST, were reproduced at both of mRNA (28.8 ± 4.7% of the control) and protein (69.5 ± 4.7% of the control) levels (Fig. 1G, H). We then examined the effects of paroxetine on the LPS-induced decrease in the L-Glu transporter expression. Paroxetine significantly prevented the decreases at both of mRNA (28.8 ± 4.7 to 49.6 ± 3.3%; $n = 10$) and protein (from 69.5 ± 4.7% to 91.0 ± 5.1%; $n = 5$) levels (Fig. 1G, H). As is shown in Fig. 1, fluvoxamine and sertraline, the other SSRIs in this study, did not affect the decrease in L-Glu transport activity, suggesting that paroxetine revealed the effects through the mechanisms independent of its inhibitory effect on serotonin selective transporter. In support of this, LPS-induced decrease in L-Glu transport activity was not changed by the elevation of extracellular serotonin concentration (Fig. 2A). We also confirmed that paroxetine did not directly affect the L-Glu transport activity of the astrocyte culture (Fig. 2B). In our previous report, the down-regulation of GLAST in the inflammation model was caused by the elevation of extracellular L-Glu released from microglia (8). We therefore compared the effects of the antidepressants on LPS-induced L-Glu release from microglia. When microglia culture was treated with 10 ng/ml LPS for 24 h in the presence or absence of the antidepressants, only paroxetine suppressed L-Glu release in a concentration-dependent manner (Fig. 3A). The other antidepressants had no effects (Fig. 3B–E). We confirmed that paroxetine did not affect the microglial viability until 10 μM by LDH assay (data not shown). These results strongly suggest that the protective effect of paroxetine on the LPS-induced down-regulation of astrocytic L-Glu transporters was caused by the suppression of L-Glu release from microglia.

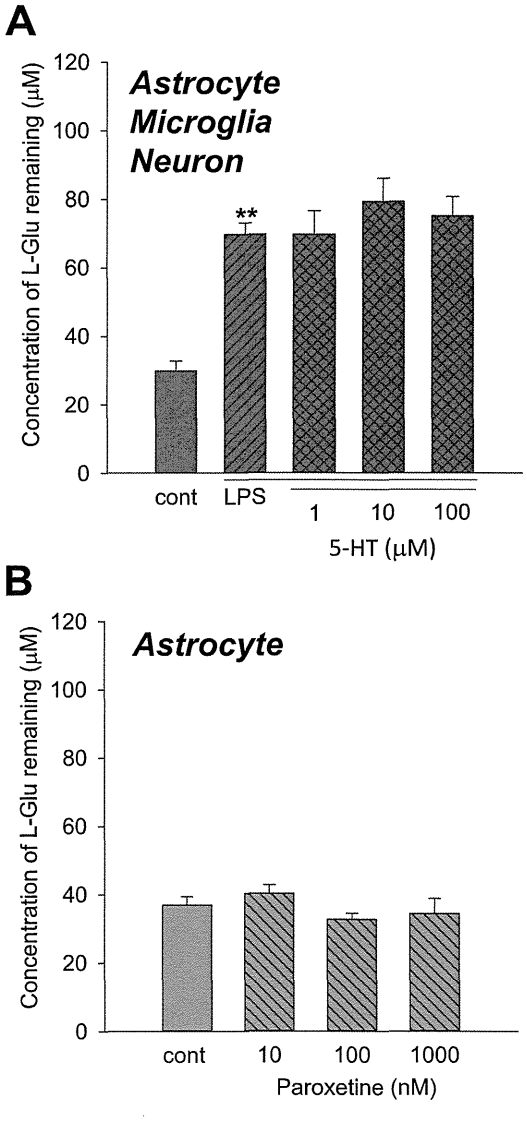

Fig. 2. Relation of the effects of paroxetine on LPS-induced decrease in L-Glu transport activity with its SSRI function and the direct effect on astrocytes. A. 72 h treatment with 5-HT (1–100 μM) did not affect LPS-induced decrease in the L-Glu transport activity. B. 72 h treatment with paroxetine (10–1000 nM) of astrocyte culture did not affect its L-Glu transport activity. **: $p < 0.01$ vs. control group, Tukey's test following ANOVA ($N = 6$).

The shape of microglia in the mixed culture was dramatically changed to amoeboid type by LPS and this morphological change was remarkably suppressed by paroxetine (unpublished observation). This suggests that paroxetine does not only suppress L-Glu release from microglia alone but also microglial activation. To demonstrate this possibility, the effect of paroxetine on the microglial activation is needed to be confirmed using multiple parameters. Because SSRIs have diverse chemical structures despite a common mode of action of 5-HT function (11), it is possible that paroxetine revealed the effects through interaction with paroxetine-specific target molecules. Because paroxetine exhibited the powerful inhibition of calcium influx via $P2X_4$ receptors (12), $P2X_4$ receptor is one of the most probable candidate molecules. The expression level of $P2X_4$ receptor in microglia is up-regulated in inflammatory pain model in spinal cord and is thought to be important for microglial inflammatory responses (13). MAPK signaling molecules (14) and GABA(B) receptor (15) are possibly involved in the paroxetine-specific effects as well. The effective concentration of paroxetine to reduce L-Glu release was 1 μM. According to the attached documents of paroxetine (http://www.info.pmda.go.jp/), intracerebral concentration of paroxetine reaches 77 nM by 25 mg/day-repeated administration. It is therefore unlikely that paroxetine affects astrocyte L-Glu transporters and microglia by the general dosage of SSRI. For clinical application of our present findings, further investigation concerning application period and dosage is needed.

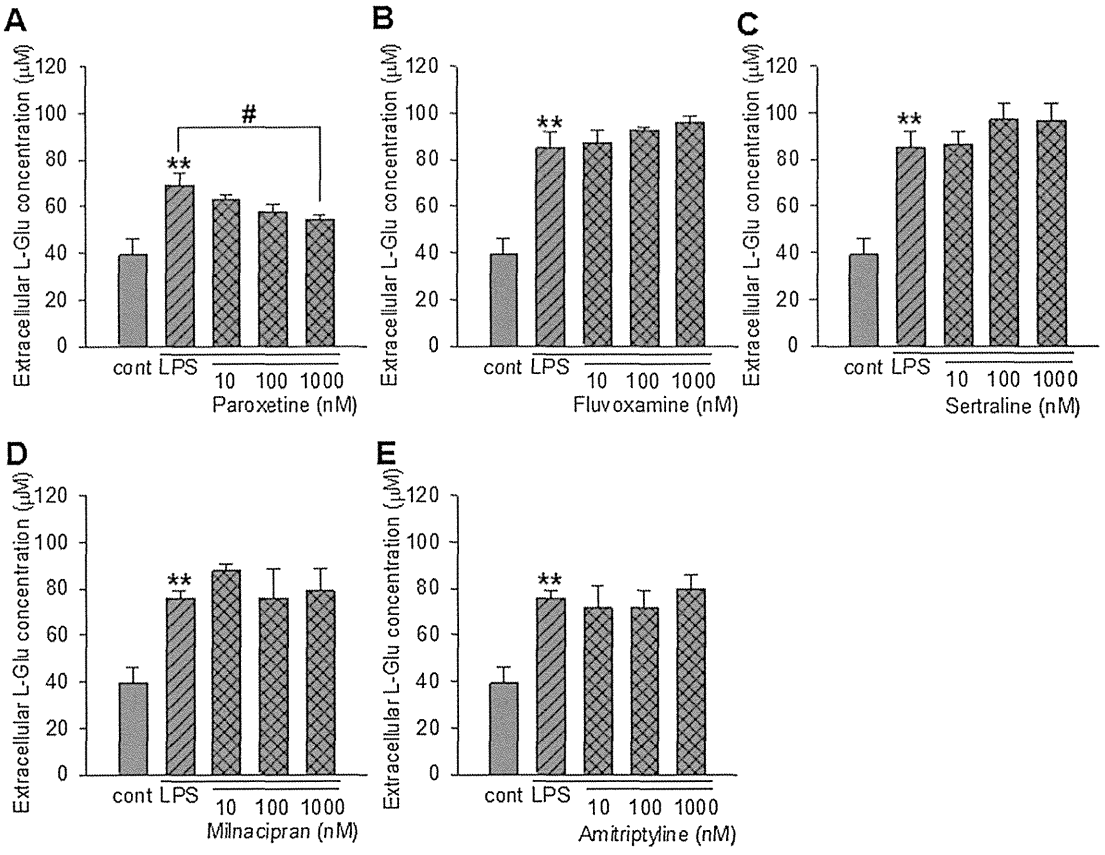

Fig. 3. Effects of antidepressants on the L-Glu release from microglia under the inflammatory condition. In each set of experiment, antidepressants were applied to the mixed culture from 1 h before to the end of the LPS-treatment (10 ng/ml, 24 h). The extracellular concentration of L-Glu was quantified. Paroxetine prevented the LPS-induced L-Glu release from microglia in a concentration-dependent manner (A). Fluvoxamine (B), sertraline (C), milnacipran (D), and amitriptyline (E) had no effects on LPS-induced L-Glu release from microglia. **: $p < 0.01$ vs. control group, #: $p < 0.05$ vs. LPS-treated group, Tukey's test following ANOVA ($N = 6$).

In conclusion, we found that paroxetine inhibit the L-Glu release from activated microglia and prevent down-regulation of astrocytic L-Glu transporters in the early stage of neuroinflammation. This is the novel pharmacological effect of paroxetine, which may bring advantages on the therapy of the disease associated with neuroinflammation.

Conflicts of interest

I declare that I have no significant competing financial, professional or personal interests that might have influenced the results and interpretation of the manuscript.

Author's contributions

K.F. performed experiments and manuscript writing.
J.T. performed experiments.
Y.S-M. provided advice on manuscript writing
Y.S. provided advice on manuscript writing
T.S. provided advice on the experimental direction and manuscript writing.
K.S. designed the experimental plan and performed experiments, manuscript writing.

Acknowledgments

This work was partly supported by a Grant-in-Aid for Young Scientists from Ministry of Education, Culture, Sports, Science, and Technology, Japan (KAKENHI 21700422), the Program for Promotion of Fundamental Studies in Health Sciences of National Institute of Biomedical Innovaton (10-21), Japan, a Health and Labor Science Research Grant for Research on Risks of Chemicals, a Labor Science Research Grant for Research on New Drug Development from the MHLW, Japan, awarded to K.S., Grant-in-Aid for research from MEXT, Japan (KAKENHI C23590113) awarded to T.S., and a Health and Labor Science Research Grant for Research on Publicly Essential Drugs and Medical Devices, Japan, awarded to Y.S.

References

(1) Bowerman M, Vincent T, Scamps F, Perrin FE, Camu W, Raoul C. Neuroimmunity dynamics and the development of therapeutic strategies for amyotrophic lateral sclerosis. Front Cell Neurosci. 2013;7:214.
(2) Liimatainen S, Lehtimaki K, Palmio J, Alapirtti T, Peltola J. Immunological perspectives of temporal lobe seizures. J Neuroimmunol. 2013;263:1–7.
(3) Schwartz M, Baruch K. The resolution of neuroinflammation in neurodegeneration: leukocyte recruitment via the choroid plexus. EMBO J. 2014;33:7–22.
(4) Lucas SM, Rothwell NJ, Gibson RM. The role of inflammation in CNS injury and disease. Br J Pharmacol. 2006;147(Suppl. 1):S232–S240.
(5) Masliah E, Alford M, DeTeresa R, Mallory M, Hansen L. Deficient glutamate transport is associated with neurodegeneration in Alzheimer's disease. Ann Neurol. 1996;40:759–766.
(6) Ferrarese C, Zoia C, Pecora N, Piolti R, Frigo M, Bianchi G, et al. Reduced platelet glutamate uptake in Parkinson's disease. J Neural Transm. 1999;106:685–692.
(7) Rothstein JD, Martin LJ, Kuncl RW. Decreased glutamate transport by the brain and spinal cord in amyotrophic lateral sclerosis. N Engl J Med. 1992;326:1464–1468.
(8) Takaki J, Fujimori K, Miura M, Suzuki T, Sekino Y, Sato K. L-glutamate released from activated microglia downregulates astrocytic L-glutamate transporter

expression in neuroinflammation: the 'collusion' hypothesis for increased extracellular L-glutamate concentration in neuroinflammation. J Neuroinflammation. 2012;9:275.
(9) Hashioka S, Klegeris A, Monji A, Kato T, Sawada M, McGeer PL, et al. Antidepressants inhibit interferon-gamma-induced microglial production of IL-6 and nitric oxide. Exp Neurol. 2007;206:33–42.
(10) Hwang J, Zheng LT, Ock J, Lee MG, Kim SH, Lee HW, et al. Inhibition of glial inflammatory activation and neurotoxicity by tricyclic antidepressants. Neuropharmacology. 2008;55:826–834.
(11) RJ B. Drugs and the treatment of psychiatrc disorders. Goodman and Gilman's the pharmacological basis of therapeutics. In: Hardman JG, Limbird LE, Gilman AG, editors. 10th ed 2001. p. 447–483.
(12) Nagata K, Imai T, Yamashita T, Tsuda M, Tozaki-Saitoh H, Inoue K. Antidepressants inhibit P2X4 receptor function: a possible involvement in neuropathic pain relief. Mol Pain. 2009;5:20.
(13) Guo LH, Trautmann K, Schluesener HJ. Expression of P2X4 receptor by lesional activated microglia during formalin-induced inflammatory pain. J Neuroimmunol. 2005;163:120–127.
(14) Liu RP, Zou M, Wang JY, Zhu JJ, Lai JM, Zhou LL, et al. Paroxetine ameliorates lipopolysaccharide-induced microglia activation via differential regulation of MAPK signaling. J Neuroinflammation. 2014;11:47.
(15) Khundakar AA, Zetterstrom TS. Effects of GABAB ligands alone and in combination with paroxetine on hippocampal BDNF gene expression. Eur J Pharmacol. 2011;671:33–38.

Fundamental Toxicological Sciences (Fund. Toxicol. Sci.)
Vol.1, No.3, 87-94, 2014

Original Article

Residual metals in carbon nanotubes suppress the proliferation of neural stem cells

Yukari Shigemoto-Mogami[1], Koki Fujimori[1,2], Yoshiaki Ikarashi[3], Akihiko Hirose[4], Yuko Sekino[1] and Kaoru Sato[1]

[1]*Laboratory of Neuropharmacology, Division of Pharmacology, National Institute of Health Sciences, 1-18-1 Kamiyoga, Setagaya-ku, Tokyo 158-8501, Japan*
[2]*Division of Basic Biological Science, Faculty of Pharmacy, Keio University, 1-5-30 Shiba-koen, Minato-ku, Tokyo 105-8512, Japan*
[3]*Division of Environmental Chemistry, National Institute of Health Sciences, 1-18-1 Kamiyoga, Setagaya-ku, Tokyo 158-8501, Japan*
[4]*Division of Risk Assessment, National Institute of Health Sciences, 1-18-1 Kamiyoga, Setagaya-ku, Tokyo 158-8501, Japan*

(Received October 17, 2014; Accepted October 20, 2014)

ABSTRACT — Carbon nanotubes (CNTs) are used in many fields; however, little is known about the effects of CNTs on the central nervous system (CNS). In this study, we found that extracts of sonicated CNTs suppressed the proliferation of neural stem cells (NSCs). Single-walled CNTs (SWCNTs) and multiple-walled CNTs (MWCNTs) were suspended in PBS (1 mg/mL) and sonicated for 5 hr using a water bath sonicator. Supernatants from both types of CNTs suppressed NSC proliferation. The effects weakened in a dilution-ratio-dependent manner and strengthened in a sonication time-dependent manner. Metal concentrations extracted from SCNTs and MCNTs after 5-hr of sonication were determined using inductively coupled plasma mass spectrometry. Mn, Rb, Cs, Tl, and Fe were detected in the SWCNT supernatant, and Mn, Cs, W, and Tl were detected in the MWCNT supernatant. The concentration of Mn, Rb, and Fe eluted from the SWCNTs and Rb eluted from MWCNTs following sonication were sufficient to suppress NSC proliferation alone. N-acetyl cysteine (NAC) and ascorbic acid (AA) reversed the effects of Mn and Fe and restored NSC proliferation. The effects of Rb and Tl were not affected by the antioxidants. Both antioxidants largely restored the suppression of NSC proliferation induced by the SWCNT and MWCNT supernatants. These results suggest that metals extracted from CNTs via a strong vibration energy can suppress NSC proliferation through ROS production by the extracted metals.

Key words: Carbon nanotube, Neural stem cell, Metals, Proliferation

INTRODUCTION

CNTs are fiber-shaped nanomaterials that consist of graphite hexagonal-mesh planes (graphene sheet) in a single-layer (single-walled carbon nanotubes (SWCNTs)) or in multiple layers with nest accumulation (multi-walled carbon nanotubes (MWCNTs)). The structure of SWCNTs is a honeycomb carbon lattice rolled into a cylinder, and the basic morphology consists of a sheet of tangled SWCNT (with a diameter of approximately 2 nm) bundles with diameters tens of nanometers in length. The structure of MWCNTs consists of honeycomb carbon lattices rolled into a multi-layer tubular shape, and the basic morphology is composed of particles of tangled MWCNTs with a diameter of approximately 30 nm. CNTs are used in many fields, including energy, healthcare, environment, materials, and electronics. However, adverse effects of CNTs on human health are poorly understood. Exposure to asbestos is known to cause asbestosis, bronchogenic carcinoma, mesothelioma, pleural fibrosis and pleural plaques, indicating that both the lungs and the pleura are targets of asbestos (Donaldson *et al.*, 2013). CNTs also exist as fibers or compact particles; thus, most studies concerning the adverse effects of CNTs have focused on lung toxicity (Jaurand *et al.*, 2009; Pacurari *et al.*, 2010) based on the fiber pathogenicity paradigm developed in the 1970-80s.

Correspondence: Kaoru Sato (E-mail: kasato@nihs.go.jp)

However, recent reports showed that nano-particles can cross the blood–brain barrier (BBB) and enter the brain (Sharma and Sharma, 2007). Furthermore, it has been suggested that the olfactory nerve pathway is a portal of entry into the CNS (Henriksson and Tjalve, 2000; Persson *et al.*, 2003; Mistry *et al.*, 2009; Balasubramanian *et al.*, 2013). Recent reports showed that MWCNTs are toxic to neural cells (Belyanskaya *et al.*, 2009; Xu *et al.*, 2009; Gavello *et al.*, 2012). Here, we investigated the effects of CNTs on the self-renewal of neural stem cells (NSCs). The mammalian CNS comprises various cell types, including neurons, astrocytes, and oligodendrocytes, and these cells differentiate from NSCs at specific brain developmental stages. Sufficient proliferation of NSCs before differentiation is essential to supply the neurons and glia required for brain function (Caviness *et al.*, 1995; Kriegstein and Alvarez-Buylla, 2009). In addition, NSCs are maintained in the subventricular zone and the hippocampal subgranular zone in the adult brain. Adult neurogenesis from these NSCs plays a key role in higher-order brain functions, such as cognition, learning and memory (Couillard-Despres *et al.*, 2011; Eisch and Petrik, 2012; Rolando and Taylor, 2014). Thus, the effects of CNTs on the proliferation of NSCs need to be determined for both of brain development and brain function. Here, we report that sonicated extracts of CNTs suppressed the proliferation of NSCs. We also determined that these effects were mediated through ROS produced by residual metals in the CNTs.

MATERIALS AND METHODS

Materials

CNTs (SWCNT: purity > 95%; Lot No.: SW1859; MWCNT: purity: > 98%; Lot No.: 04-12/10#1-(4)) were supplied by Nikkiso Co., Ltd. (Shizuoka, Japan). Both test materials were not coated or modified. The detailed physiochemical properties of Nikkiso CNTs have been previously reported (Ema *et al.*, 2011; Matsumoto *et al.*, 2012). Epidermal growth factor (EGF), $MnCl_2$, RbCl, $TlCl_3$, $FeCl_2$, $FeCl_3$, and NAC were purchased from Sigma (St. Louis, Mo, USA). Fibroblast growth factor 2 (FGF2) was purchased from PeproTech (Rocky Hill, NJ, USA). AA was purchased from WAKO (Osaka, Japan). The BrdU cell proliferation assay kit was purchased from Merck (Darmstadt, Germany). B27 supplement, TrypLE Select, FBS, and DMEM were purchased from Life Technologies (Grand Island, NY, USA).

Preparation of supernatants of sonicated CNT solutions

SWCNTs and MWCNTs were suspended in PBS (1 mg/mL) and sonicated for 10 min or 5 hr using a water bath-sonicator (Hitachi-Kokusai Electric Inc., Tokyo, Japan) at a frequency of 36 kHz and a watt density of 65 W/264 cm^2. The supernatants of sonicated CNT suspensions were diluted with culture medium 10- to 1,000-fold.

Rat neural stem cell (NSC) culture

Rat NSCs were cultured as previously described (Reynolds *et al.*, 1992; Hamanoue *et al.*, 2009) with slight modifications. Briefly, the telencephalons were dissected from embryonic day 16 (E16) rats of either sex in ice-cold DMEM/F12. The tissue was then minced and dispersed into single cells by pipetting. Cells were then cultured in DMEM/F12 containing B27 supplement (1/200), 20 ng/mL fibroblast growth factor 2 (FGF2) and 20 ng/mL epidermal growth factor (EGF) for 7 days. The primary neurospheres were incubated with TrypLE Select for 15 min and dissociated by pipetting. Single cells were seeded in 96-well plates for the proliferation assay.

Measurement of metal concentrations

CNTs were suspended in PBS (1 mg/mL) and sonicated for 5 hr using a water bath sonicator. The metal concentrations in the CNT supernatants were quantified using an inductively coupled plasma mass spectrometer (ICP-MS) (Agilent 7500ce ICP-MS, Agilent Technologies, Santa Clara, CA, USA) fitted with a collision/reaction cell in helium mode. We first detected metals at concentrations exceeding the detection limits using a semi-quantitative analysis. Next, we determined the concentration of the detected metals (i.e., Mn, Fe, Rb, Cs, W, and TI) using a full quantitative analysis with calibration curves.

Treatment of NSCs with the supernatants of sonicated CNT suspensions, metals, and antioxidants

NSCs were treated with the supernatants of sonicated CNT suspensions, $MnCl_2$ (1-100 ppb), RbCl (1-100 ppb), $TlCl_3$ (0.1-10 ppb), $FeCl_2$ (100-10,000 ppb) or $FeCl_3$ (100-10,000 ppb) with or without 10 μM N-acetyl cysteine (NAC) or 10 μM ascorbic acid (AA) for 24 hr.

NSC proliferation assay

We quantified NSC proliferation according the instructions from the BrdU cell proliferation assay kit (Calbiochem, Hayward, CA, USA). The primary neurospheres were dissociated into single cells and seeded in 96-well plates at a density of 2 x 10^4 cells/

well. BrdU was added to the medium during the treatment of NSCs. After incubation, the cells were fixed, and BrdU-immuno-labeling was performed. The fluorescence intensities were used as a marker of proliferation. The fluorescence was measured at an excitation wavelength of 320 nm and emission wavelength of 460 nm with a fluorescence microplate reader (Spectra Max Microplate reader, Molecular Devices, Sunnyvale, CA, USA).

Data analysis and statistics

All data are shown as the mean ± S.E.M. The statistical analysis was performed using Student's *t*-test or an ANOVA followed by a Tukey's test. Differences were considered to be significant at $p < 0.05$.

RESULTS

SWCNTs and MWCNTs were suspended in PBS (1 mg/mL) and sonicated for 5 hr using a water bath sonicator. The supernatants of the sonicated CNT suspensions were collected and diluted with culture medium 10- to 1,000-fold. We found that a 24-hr treatment with supernatants of SWCNT and MWCNT suppressed NSC proliferation in a dilution ratio-dependent manner (Fig. 1). The suppression of proliferation was stronger with the SWCNT supernatant when compared with the MWCNT supernatant. The effects of sonication time were also assessed. The suppressive effects of both supernatants disappeared when the sonication time was changed from 5 hr to 10 min (Fig. 2). These results suggest that the suppression of NSC proliferation is due to factors released from CNTs in a sonication time-dependent manner.

CNTs are manufactured using metallic catalysts (Ding *et al.*, 2008; Yazyev and Pasquarello, 2008; Banhart, 2009; Tyagi *et al.*, 2011). Thus, we speculated that residual metals extracted from CNTs during the 5-hr sonication may be responsible for the suppression of NSC proliferation. We therefore quantified the metal contents in the CNT supernatants. The metals in the SWCNT and MWCNT supernatants were first analyzed using ICP-MS in a semi-quantitative mode. Next, the concentrations of metals were determined using calibration curves (Table 1). We found that a 5-hr sonication induced the extraction of multiple metals from the CNTs. Mn, Rb, Cs, Tl, and Fe were detected in the SWCNT supernatant, whereas Mn, Cs, W, and Tl were detected in the MWCNT supernatant. Among these metals, the concentration of Fe in SWCNT supernatant was remarkably high (from N.D. to 7,110 ppb). The concentrations of these metals in PBS were largely negligible and did not change after a 5-hr sonication.

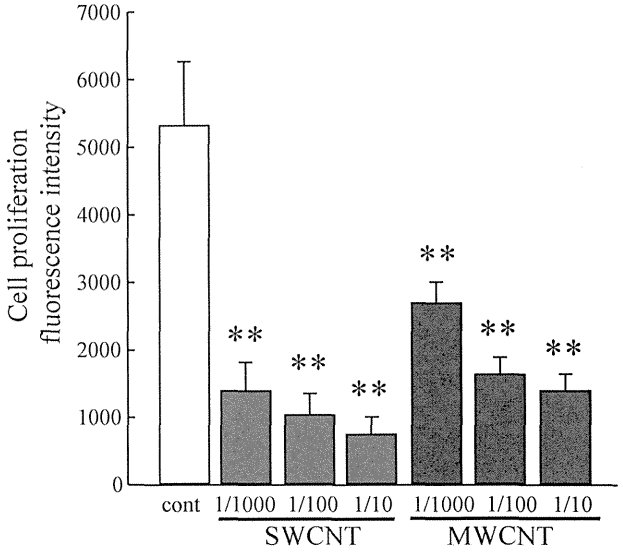

Fig. 1. Effects of the supernatants of sonicated CNT suspensions on the proliferation of rat NSCs. The supernatants of SWCNTs and MWCNTs suppressed NSC proliferation in a dilution ratio-dependent manner. *: $p < 0.05$, **: $p < 0.01$ vs. control group ($N = 6$), ANOVA followed by a Tukey's test.

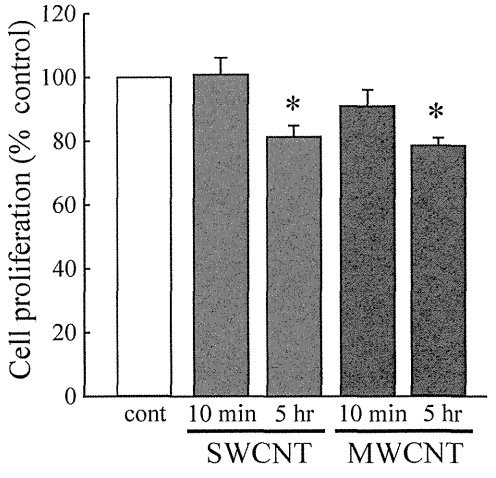

Fig. 2. Sonication time-dependence of CNT supernatant effects. The effects of SWCNT and MWCNT supernatants disappeared with a sonication time of 10 min. However, a 5-hr sonication time produced a significant suppression of NSC proliferation. *: $p < 0.05$ vs. control group ($N = 6$), ANOVA followed by a Tukey's test.

Next, we examined the direct effects of the metals at concentration ranges detected in the supernatants. Fig. 3 shows the metals that had a suppressive effect on NSC

Table 1. Metals eluted from CNTs by sonication for 5 hr.

	Concentrations of metals (ppb) 1 ppb = 10^{-8}%					
	PBS	PBS	SWCNT	SWCNT	MWCNT	MWCNT
sonication	-	+	-	+	-	+
Mn	nd	nd	0.33	16.04	nd	0.26
Rb	3.97	3.84	6.88	13.33	4.06	4.61
Cs	nd	nd	0.1	0.32	nd	0.59
W	nd	0.05	nd	0.08	nd	0.4
Tl	md	nd	0.05	0.17	nd	0.37
Fe	nd	nd	nd	7110	nd	nd

The metal concentrations in the supernatant of SWCNT and MWCNT were quantified using ICP-MS in a semi-quantitative mode followed by a full quantitative mode. Mn, Rb, Cs, W, Tl, and Fe were detected in the SWCNT supernatant. Mn, Rb, Cs, W, Tl, and Fe were detected in the MWCNT supernatant. The concentration of Fe in the SWCNT supernatant was remarkably high (7,110 ppb).

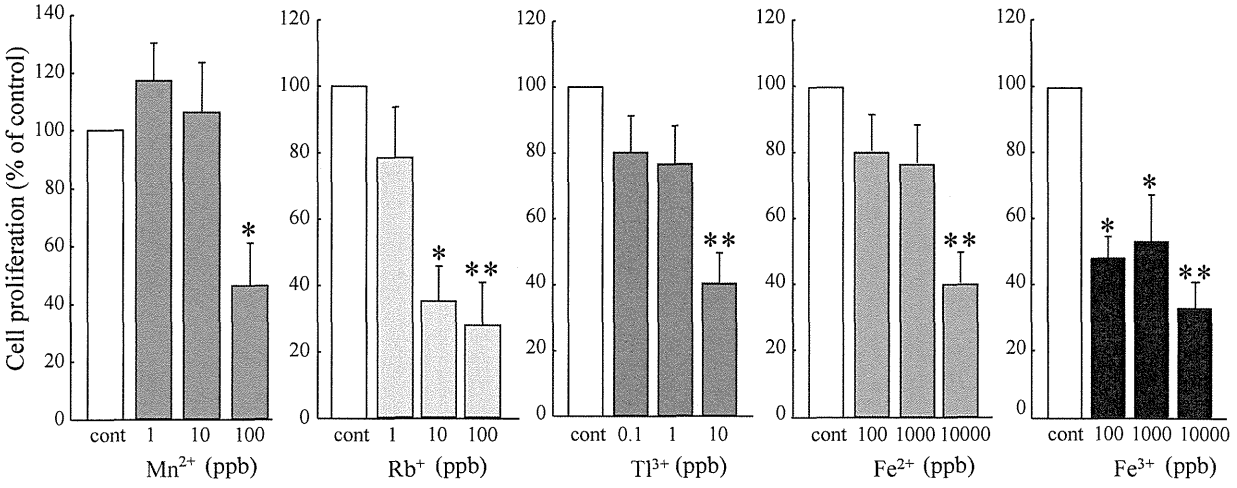

Fig. 3. The direct effect of metals in CNT supernatants. Mn^{2+}, Rb^{+}, Tl^{3+}, Fe^{2+}, and Fe^{3+} suppressed NSC proliferation in a concentration-dependent manner. *: $p < 0.05$, **: $p < 0.01$ vs. control group (N = 12), ANOVA followed by a Tukey's test.

proliferation (Fig. 3). Mn^{2+}, Rb^{+}, Tl^{3+}, Fe^{2+}, and Fe^{3+} suppressed the proliferation of NSCs in a concentration-dependent manner. These results indicate that Mn, Rb, and Fe were present in the SWCNT supernatant at a concentration high enough to suppress NSC proliferation. This effect was induced by the Rb in the MWCNT supernatant. Some metals are known to produce reactive oxygen species (Ding *et al.*, 2008) that can result in oxidative stress on lipids, DNA and proteins (Henriksson and Tjalve, 2000; Choi *et al.*, 2007; Alekseenko *et al.*, 2008; Kim *et al.*, 2011; Latronico *et al.*, 2013; Roth and Eichhorn, 2013; Sripetchwandee *et al.*, 2013). Thus, we examined the involvement of ROS in the suppression of NSC proliferation. N-acetyl cysteine (NAC) (10 μM) and ascorbic acid (AA) (10 μM) are typical antioxidants that can significantly restore the suppression of the NSC proliferation caused by Mn^{2+}, Fe^{2+}, and Fe^{3+} (Fig. 4A). The effect of Rb and Tl were not affected by NAC or AA (data not shown). These results suggest that ROS is involved in the suppressive effects produced by Mn and Fe. We also examined whether ROS played a role in the suppression of NSC proliferation by the CNT supernatants (Fig. 4B). Both NAC and AA markedly restored the decrease in NSC proliferation caused by the SWCNT and MWCNT supernatants. We confirmed that both of these antioxidants alone did not affect NSC proliferation (data not shown). Taken together, these results suggest that the suppressive effects of the sonicated extract of CNTs were mainly caused by

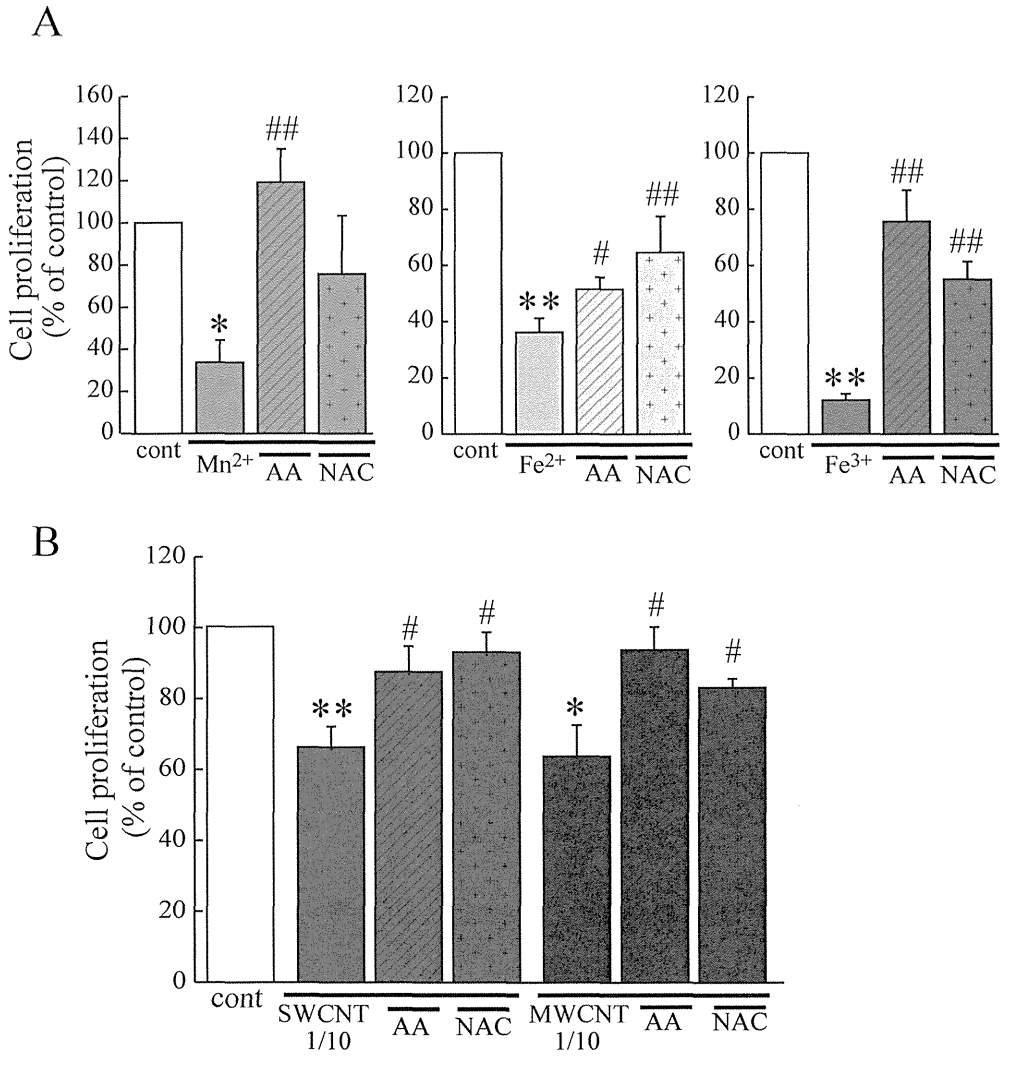

Fig. 4. Antioxidants attenuated the reduction in NSC proliferation caused by metals and CNT supernatants. The suppression of the NSC proliferation caused by Mn^{2+}, Fe^{2+}, Fe^{3+} (A) and the supernatants of CNTs (B) was significantly restored by NAC (10 μM) and AA (10 μM). *: $p < 0.05$,**: $p < 0.01$ vs. control group, #: $p < 0.05$, ##: $p < 0.01$ vs. metal or CNT-supernatant-treated groups (N = 7), ANOVA followed by a Tukey's test.

ROS produced by residual metals.

DISCUSSION

We found that the supernatants of sonicated CNT suspensions suppress NSC proliferation. We also determined that these effects were largely mediated by ROS production from residual metals. To demonstrate the involvement of ROS, we used the two antioxidants NAC and AA. NAC exerts its protective by increasing glutathione levels (Yim *et al.*, 1994; Arfsten *et al.*, 2007; Li *et al.*, 2009), directly scavenging ROS, and activating ERK1/2 (Zhang *et al.*, 2011). AA is a powerful water-soluble antioxidant that acts by scavenging ROS and reactive nitrogen species (Carr and Frei, 1999; Kojo, 2004). The concentrations of NAC and AA used in this study were at a level shown to suppress the effects of ROS in previous studies (Carr and Frei, 1999; De la Fuente and Victor, 2001; Nakajima *et al.*, 2009).

Proliferative NSCs have a high endogenous ROS lev-

el (Le Belle *et al.*, 2011), and redox balance is important to regulate NSC/neural progenitor cell (NPC)-self-renewal and differentiation (Smith *et al.*, 2000; Li *et al.*, 2007; Hou *et al.*, 2012; Topchiy *et al.*, 2013). For example, mitochondrial superoxide negatively regulates NPC-self-renewal in the developmental cerebral cortex (Hou *et al.*, 2012). High levels of ROS inhibit O-2A progenitor proliferation (Smith *et al.*, 2000; Li *et al.*, 2007). In other cases, NADPH oxidase (Nox) 4-generated superoxide drives mouse NSC proliferation (Topchiy *et al.*, 2013). Ketamine-induced ROS enhanced the proliferation of NSCs derived from human embryonic stem cells (Bai *et al.*, 2013). The effect of ROS on NSC/NPC proliferation may change depending on the subcellular localization of the ROS generation and the timing of the ROS generation.

The suppression of NSC proliferation by the supernatants of both CNTs were virtually restored by the antioxidants, suggesting that the effects of CNT-supernatants were mediated through ROS stress. After a 5-hr sonication, multiple metals were detected in the SWCNT and MWCNT supernatants using ICP-MS. Mn, Rb, Cs, Tl, and Fe were detected in the SWCNT supernatant, and Mn, Cs, W, and Tl were detected in the MWCNT supernatant. Out of these SWCNT metals, the effects of Mn and Fe were reversed by antioxidants, suggesting that Mn and Fe play the main role in the suppression of NSC proliferation by CNT supernatants. In the MWCNT supernatant, the concentrations of Mn and Fe were insufficient to suppress NSC proliferation. Thus, a combination of ROS produced by multiple metals might produce synergistic suppressive effects.

Fe is essential for biological processes, but it is also known to be toxic in excess. Fe^{2+} overload into the cells and shuttling of Fe^{2+} to Fe^{3+} leads to cellular malfunctions due to ROS production (Halliwell and Gutteridge, 1992; Touati, 2000). Although Fe^{3+} has been largely considered as non-cytotoxic (Braun, 1997; Bruins *et al.*, 2000), it has its own mechanisms that can alter cell viability (Chamnongpol *et al.*, 2002). Fe^{3+} shows ROS production even while bound to proteins (Alekseenko *et al.*, 2008). GSH revealed pro-oxidant effects in the presence of an exogenous Fe^{3+} (Zager and Burkhart, 1998). Furthermore, Fe^{2+} and Fe^{3+} were shown to enter brain mitochondria and cause mitochondrial depolarization and ROS production (Sripetchwandee *et al.*, 2013). Mn is also essential for biological processes, but it has been known to be a neurotoxicant in excess. Mn induces oxidative stress (Choi *et al.*, 2007; Park and Park, 2010) and the release of cytokines (Park and Park, 2010). Mn further potentiates inflammation by the release of MMP9 through ROS production and modulation of ERK (Latronico *et al.*, 2013). Rb was also detected in the supernatants of SWCNT and MWCNT. Here, we found that Rb alone suppressed NSC proliferation in a ROS-independent manner. Rb has long been considered as nontoxic. Rb is generally used as a medical contrast medium because of its long half-life. Thus, the mechanism behind the Rb effects should be clarified quickly.

Most commercial CNTs contain ultrafine metal particles composed of Fe, Ni, Y, Co, Pb, and Cu that are used as catalysts (Ding *et al.*, 2008; Yazyev and Pasquarello, 2008; Banhart, 2009; Tyagi *et al.*, 2011). Recent studies showed that metal impurities play a major role in CNT cytotoxicity (Liu *et al.*, 2008; Kim *et al.*, 2010). The residual metals can remain in the contact solvent or embed inside the CNTs (Pumera, 2007; Fubini *et al.*, 2011; Aldieri *et al.*, 2013). In our study, the content of Fe in SWCNT was remarkable. A SWCNT is a graphene sheet protected metal core/shell of nanoparticles (Pumera, 2007). This structure may have caused the higher levels of metal impurities when compared with MWCNTs. Our data suggest that the residual metallic catalysts are released by vibration energy with a sonication frequency of 36 kHz, watt density of 65 W/264 cm^2 and sonication time of 5 hr. Pumera *et al.* indicated that washing with concentrated nitric acid removed up to 88% (w/w) of metal catalyst nanoparticles (Pumera, 2007). For public health and the safer applications of CNTs in nano-medicine, it is preferable to decrease the amount of the metal impurities by improving the washing process.

Conflict of interest---- The authors declare that there is no conflict of interest.

REFERENCES

Aldieri, E., Fenoglio, I., Cesano, F., Gazzano, E., Gulino, G., Scarano, D., Attanasio, A., Mazzucco, G., Ghigo, D. and Fubini, B. (2013): The role of iron impurities in the toxic effects exerted by short multiwalled carbon nanotubes (MWCNT) in murine alveolar macrophages. J. Toxicol. Environ. Health Part A, **76**, 1056-1071.

Alekseenko, A.V., Waseem, T.V. and Fedorovich, S.V. (2008): Ferritin, a protein containing iron nanoparticles, induces reactive oxygen species formation and inhibits glutamate uptake in rat brain synaptosomes. Brain Res., **1241**, 193-200.

Arfsten, D.P., Johnson, E.W., Wilfong, E.R., Jung, A.E. and Bobb, A.J. (2007): Distribution of radio-labeled N-Acetyl-L-Cysteine in Sprague-Dawley rats and its effect on glutathione metabolism following single and repeat dosing by oral gavage. Cutan. Ocul. Toxicol., **26**, 113-134.

Bai, X., Yan, Y., Canfield, S., Muravyeva, M.Y., Kikuchi, C., Zaja, I., Corbett, J.A. and Bosnjak, Z.J. (2013): Ketamine enhances human neural stem cell proliferation and induces neuronal apop-

tosis via reactive oxygen species-mediated mitochondrial pathway. Anesth. Analg., **116**, 869-880.

Balasubramanian, S.K., Poh, K.W., Ong, C.N., Kreyling, W.G., Ong, W.Y. and Yu, L.E. (2013): The effect of primary particle size on biodistribution of inhaled gold nano-agglomerates. Biomaterials, **34**, 5439-5452.

Banhart, F. (2009): Interactions between metals and carbon nanotubes: at the interface between old and new materials. Nanoscale, **1**, 201-213.

Belyanskaya, L., Weigel, S., Hirsch, C., Tobler, U., Krug, H.F. and Wick, P. (2009): Effects of carbon nanotubes on primary neurons and glial cells. Neurotoxicology, **30**, 702-711.

Braun, V. (1997): Avoidance of iron toxicity through regulation of bacterial iron transport. Biol. Chem., **378**, 779-786.

Bruins, M.R., Kapil, S. and Oehme, F.W. (2000): Microbial resistance to metals in the environment. Ecotoxicol. Environ. Saf., **45**, 198-207.

Carr, A. and Frei, B. (1999): Does vitamin C act as a pro-oxidant under physiological conditions? FASEB J., **13**, 1007-1024.

Caviness, V.S.Jr., Takahashi, T. and Nowakowski, R.S. (1995): Numbers, time and neocortical neuronogenesis: a general developmental and evolutionary model. Trends Neurosci., **18**, 379-383.

Chamnongpol, S., Dodson, W., Cromie, M.J., Harris, Z.L. and Groisman, E.A. (2002): Fe(III)-mediated cellular toxicity. Mol. Microbiol., **45**, 711-719.

Choi, C.J., Anantharam, V., Saetveit, N.J., Houk, R.S., Kanthasamy, A. and Kanthasamy, A.G. (2007): Normal cellular prion protein protects against manganese-induced oxidative stress and apoptotic cell death. Toxicol. Sci., **98**, 495-509.

Couillard-Despres, S., Iglseder, B. and Aigner, L. (2011): Neurogenesis, cellular plasticity and cognition: the impact of stem cells in the adult and aging brain--a mini-review. Gerontology, **57**, 559-564.

De la Fuente, M. and Victor, V.M. (2001): Ascorbic acid and N-acetylcysteine improve *in vitro* the function of lymphocytes from mice with endotoxin-induced oxidative stress. Free Radic. Res., **35**, 73-84.

Ding, F., Larsson, P., Larsson, J.A., Ahuja, R., Duan, H., Rosen, A. and Bolton, K. (2008): The importance of strong carbon-metal adhesion for catalytic nucleation of single-walled carbon nanotubes. Nano Lett., **8**, 463-468.

Donaldson, K., Poland, C.A., Murphy, F.A., MacFarlane, M., Chernova, T. and Schinwald, A. (2013): Pulmonary toxicity of carbon nanotubes and asbestos - similarities and differences. Adv. Drug Deliv. Rev., **65**, 2078-2086.

Eisch, A.J. and Petrik, D. (2012): Depression and hippocampal neurogenesis: a road to remission? Science, **338**, 72-75.

Ema, M., Matsuda, A., Kobayashi, N., Naya, M. and Nakanishi, J. (2011): Evaluation of dermal and eye irritation and skin sensitization due to carbon nanotubes. Regul.Toxicol. Pharmacol., **61**, 276-281.

Fubini, B., Fenoglio, I., Tomatis, M. and Turci, F. (2011): Effect of chemical composition and state of the surface on the toxic response to high aspect ratio nanomaterials. Nanomedicine (Lond), **6**, 899-920.

Gavello, D., Vandael, D.H., Cesa, R., Premoselli, F., Marcantoni, A., Cesano, F., Scarano, D., Fubini, B., Carbone, E., Fenoglio, I. and Carabelli, V. (2012): Altered excitability of cultured chromaffin cells following exposure to multi-walled carbon nanotubes. Nanotoxicology, **6**, 47-60.

Halliwell, B. and Gutteridge, J.M. (1992): Biologically relevant metal ion-dependent hydroxyl radical generation. An update. FEBS Lett., **307**, 108-112.

Hamanoue, M., Matsuzaki, Y., Sato, K., Okano, H.J., Shibata, S., Sato, I., Suzuki, S., Ogawara, M., Takamatsu, K. and Okano, H. (2009): Cell surface N-glycans mediated isolation of mouse neural stem cells. J. Neurochem., **110**, 1575-1584.

Henriksson, J. and Tjalve, H. (2000): Manganese taken up into the CNS via the olfactory pathway in rats affects astrocytes. Toxicol. Sci., **55**, 392-398.

Hou, Y., Ouyang, X., Wan, R., Cheng, H., Mattson, M.P. and Cheng, A. (2012): Mitochondrial superoxide production negatively regulates neural progenitor proliferation and cerebral cortical development. Stem Cells, **30**, 2535-2547.

Jaurand, M.C., Renier, A. and Daubriac, J. (2009): Mesothelioma: Do asbestos and carbon nanotubes pose the same health risk? Part. Fibre Toxicol., **6**, 16.

Kim, J.E., Lim, H.T., Minai-Tehrani, A., Kwon, J.T., Shin, J.Y., Woo, C.G., Choi, M., Baek, J., Jeong, D.H., Ha, Y.C., Chae, C.H., Song, K.S., Ahn, K.H., Lee, J.H., Sung, H.J., Yu, I.J., Beck, G.R.Jr. and Cho, M.H. (2010): Toxicity and clearance of intratracheally administered multiwalled carbon nanotubes from murine lung. J. Toxicol. Environ. Health Part A, **73**, 1530-1543.

Kim, K.K., Singh, R.K., Strongin, R.M., Moore, R.G., Brard, L. and Lange, T.S. (2011): Organometallic iron(III)-salophene exerts cytotoxic properties in neuroblastoma cells via MAPK activation and ROS generation. PloS One, **6**, e19049.

Kojo, S. (2004): Vitamin C: basic metabolism and its function as an index of oxidative stress. Curr. Med. Chem., **11**, 1041-1064.

Kriegstein, A. and Alvarez-Buylla, A. (2009): The glial nature of embryonic and adult neural stem cells. Ann. Rev. Neurosci., **32**, 149-184.

Latronico, T., Brana, M.T., Merra, E., Fasano, A., Di Bari, G., Casalino, E. and Liuzzi, G.M. (2013): Impact of manganese neurotoxicity on MMP-9 production and superoxide dismutase activity in rat primary astrocytes. Effect of resveratrol and therapeutical implications for the treatment of CNS diseases. Toxicol. Sci., **135**, 218-228.

Le Belle, J.E., Orozco, N.M., Paucar, A.A., Saxe, J.P., Mottahedeh, J., Pyle, A.D., Wu, H. and Kornblum, H.I. (2011): Proliferative neural stem cells have high endogenous ROS levels that regulate self-renewal and neurogenesis in a PI3K/Akt-dependant manner. Cell Stem Cell, **8**, 59-71.

Li, W., Nie, S., Yu, Q. and Xie, M. (2009): (-)-Epigallocatechin-3-gallate induces apoptosis of human hepatoma cells by mitochondrial pathways related to reactive oxygen species. J. Agric. Food Chem., **57**, 6685-6691.

Li, Z., Dong, T., Proschel, C. and Noble, M. (2007): Chemically diverse toxicants converge on Fyn and c-Cbl to disrupt precursor cell function. PLoS Biol., **5**, e35.

Liu, X., Guo, L., Morris, D., Kane, A.B. and Hurt, R.H. (2008): Targeted Removal of Bioavailable Metal as a Detoxification Strategy for Carbon Nanotubes. Carbon, **46**, 489-500.

Matsumoto, M., Serizawa, H., Sunaga, M., Kato, H., Takahashi, M., Hirata-Koizumi, M., Ono, A., Kamata, E. and Hirose, A. (2012): No toxicological effects on acute and repeated oral gavage doses of single-wall or multi-wall carbon nanotube in rats. J. Toxicol. Sci., **37**, 463-474.

Mistry, A., Stolnik, S. and Illum, L. (2009): Nanoparticles for direct nose-to-brain delivery of drugs. Int. J. Pharm., **379**, 146-157.

Nakajima, Y., Tsuruma, K., Shimazawa, M., Mishima, S. and Hara, H. (2009): Comparison of bee products based on assays of antioxidant capacities. BMC Complement. Altern. Med., **9**, 4.

Pacurari, M., Castranova, V. and Vallyathan, V. (2010): Single- and multi-wall carbon nanotubes versus asbestos: are the carbon nanotubes a new health risk to humans? J. Toxicol. Environ. Health A., **73**, 378-395.

Park, E.J. and Park, K. (2010): Induction of oxidative stress and inflammatory cytokines by manganese chloride in cultured T98G cells, human brain glioblastoma cell line. Toxicol. In Vitro, **24**, 472-479.

Persson, E., Henriksson, J. and Tjalve, H. (2003): Uptake of cobalt from the nasal mucosa into the brain via olfactory pathways in rats. Toxicol. Lett., **145**, 19-27.

Pumera, M. (2007): Carbon nanotubes contain residual metal catalyst nanoparticles even after washing with nitric acid at elevated temperature because these metal nanoparticles are sheathed by several graphene sheets. Langmuir, **23**, 6453-6458.

Reynolds, B.A., Tetzlaff, W. and Weiss, S. (1992): A multipotent EGF-responsive striatal embryonic progenitor cell produces neurons and astrocytes. J. Neurosci., **12**, 4565-4574.

Rolando, C. and Taylor, V. (2014): Neural stem cell of the hippocampus: development, physiology regulation, and dysfunction in disease. Curr Top Dev Biol., **107**, 183-206.

Roth, J.A. and Eichhorn, M. (2013): Down-regulation of LRRK2 in control and DAT transfected HEK cells increases manganese-induced oxidative stress and cell toxicity. Neurotoxicology, **37**, 100-107.

Sharma, H.S. and Sharma, A. (2007): Nanoparticles aggravate heat stress induced cognitive deficits, blood-brain barrier disruption, edema formation and brain pathology. Prog. Brain Res., **162**, 245-273.

Smith, J., Ladi, E., Mayer-Proschel, M. and Noble, M. (2000): Redox state is a central modulator of the balance between self-renewal and differentiation in a dividing glial precursor cell. Proceedings of the National Academy of Sciences of the United States of America, **97**, 10032-10037.

Sripetchwandee, J., Sanit, J., Chattipakorn, N. and Chattipakorn, S.C. (2013): Mitochondrial calcium uniporter blocker effectively prevents brain mitochondrial dysfunction caused by iron overload. Life Sci., **92**, 298-304.

Topchiy, E., Panzhinskiy, E., Griffin, W.S., Barger, S.W., Das, M. and Zawada, W.M. (2013): Nox4-generated superoxide drives angiotensin II-induced neural stem cell proliferation. Dev. Neurosci., **35**, 293-305.

Touati, D. (2000): Iron and oxidative stress in bacteria. Arch. Biochem. Biophys., **373**, 1-6.

Tyagi, P.K., Janowska, I., Cretu, O., Pham-Huu, C. and Banhart, F. (2011): Catalytic action of gold and copper crystals in the growth of carbon nanotubes. J. Nanosci. Nanotechnol., **11**, 3609-3615.

Xu, L.J., Zhao, J.X., Zhang, T., Ren, G.G. and Yang, Z. (2009): *In vitro* study on influence of nano particles of CuO on CA1 pyramidal neurons of rat hippocampus potassium currents. Environ. Toxicol., **24**, 211-217.

Yazyev, O.V. and Pasquarello, A. (2008): Effect of metal elements in catalytic growth of carbon nanotubes. Phys. Rev. Lett., **100**, 156102.

Yim, M.B., Chae, H.Z., Rhee, S.G., Chock, P.B. and Stadtman, E.R. (1994): On the protective mechanism of the thiol-specific antioxidant enzyme against the oxidative damage of biomacromolecules. J. Biol. Chem., **269**, 1621-1626.

Zager, R.A. and Burkhart, K.M. (1998): Differential effects of glutathione and cysteine on Fe2+, Fe3+, H2O2 and myoglobin-induced proximal tubular cell attack. Kidney Int., **53**, 1661-1672.

Zhang, Z., Teruya, K., Eto, H. and Shirahata, S. (2011): Fucoidan extract induces apoptosis in MCF-7 cells via a mechanism involving the ROS-dependent JNK activation and mitochondria-mediated pathways. PloS One, **6**, e27441.

SCIENTIFIC REPORTS

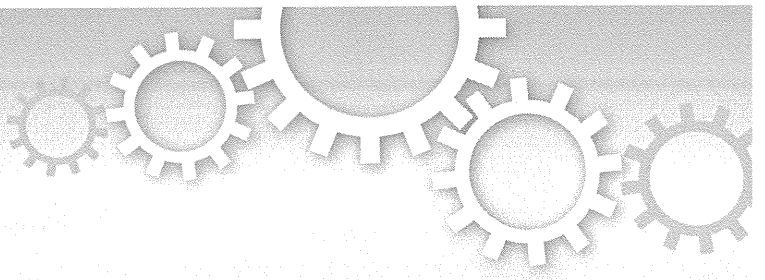

OPEN

SUBJECT AREAS:
METABOLOMICS
ENVIRONMENTAL SCIENCES

Received
17 February 2014

Accepted
15 July 2014

Published
5 August 2014

Correspondence and requests for materials should be addressed to Y.Ka (kanda@nihs.go.jp)

NAD-dependent isocitrate dehydrogenase as a novel target of tributyltin in human embryonic carcinoma cells

Shigeru Yamada[1], Yaichiro Kotake[2], Yosuke Demizu[3], Masaaki Kurihara[3], Yuko Sekino[1] & Yasunari Kanda[1]

[1]Division of Pharmacology, National Institute of Health Sciences, Tokyo, Japan, [2]Graduate School of Biomedical and Health Sciences, Hiroshima University, Hiroshima, Japan, [3]Division of Organic Chemistry, National Institute of Health Sciences, Tokyo, Japan.

Tributyltin (TBT) is known to cause developmental defects as endocrine disruptive chemicals (EDCs). At nanomoler concentrations, TBT actions were mediated by genomic pathways via PPAR/RXR. However, non-genomic target of TBT has not been elucidated. To investigate non-genomic TBT targets, we performed comprehensive metabolomic analyses using human embryonic carcinoma NT2/D1 cells. We found that 100 nM TBT reduced the amounts of α-ketoglutarate, succinate and malate. We further found that TBT decreased the activity of NAD-dependent isocitrate dehydrogenase (NAD-IDH), which catalyzes the conversion of isocitrate to α-ketoglutarate in the TCA cycle. In addition, TBT inhibited cell growth and enhanced neuronal differentiation through NAD-IDH inhibition. Furthermore, studies using bacterially expressed human NAD-IDH and in silico simulations suggest that TBT inhibits NAD-IDH due to a possible interaction. These results suggest that NAD-IDH is a novel non-genomic target of TBT at nanomolar levels. Thus, a metabolomic approach may provide new insights into the mechanism of EDC action.

Endocrine disruptive compounds (EDCs) have been studied extensively in environmental biology[1]. A large number of EDCs are known to cause genomic action via nuclear receptor. For example, xenoestrogens such as bisphenol A, genistein and diethylstilbestrol can bind to the estrogen receptor (ER) in the cell nucleus, followed by the alteration of gene expression[2,3]. In addition, EDCs induce the activation of non-genomic signaling pathways. For example, xenoestrogens increase intracellular calcium levels, activating eNOS and signaling cascades such as PI3K/AKT and MAPK[4–7]. Thus, both genomic and non-genomic pathways are required to understand the mechanism of EDC action.

Organotin compounds, such as tributyltin (TBT) are typical environmental contaminants and well known to cause developmental defects as EDCs. For example, TBT can cause increased fetal mortality, decreased fetal birth weights, and behavioral abnormalities in rat offspring[8,9]. Although the use of TBT has already been restricted, butyltin compounds, including TBT, can still be found in human blood at concentrations between 50 and 400 nM[10]. Several studies revealed that TBT activates retinoid X receptor (RXR) and/or peroxisome proliferator-activated receptor γ (PPARγ). These genomic transcriptional activations result in developmental effects, such as the imposex in many marine species[11–13] and the enhancement of adipocyte differentiation in mammals[14,15]. These TBT actions involve a higher binding affinity compared to intrinsic ligands at nM concentrations. In addition to the genomic effects, non-genomic action of TBT has been also reported. For example, TBT has been reported to inhibit the steroid biosynthesis pathway, which is responsible for the production of estrogen and androgen[16–18]. Another report has shown that TBT inhibits mitochondrial F1F0 ATP synthase[19]. These data were obtained at μM concentrations. Thus, the mechanism of nM concentrations of TBT has not been elucidated at a non-genomic level. In a previous study, we reported that treatment with 100 nM TBT resulted in growth arrest by targeting the glycolytic systems of the human embryonic carcinoma cell line NT2/D1[20]. Therefore, we raised the possibility that nM concentrations of TBT may target other non-genomic pathways which are involved in energy metabolism.

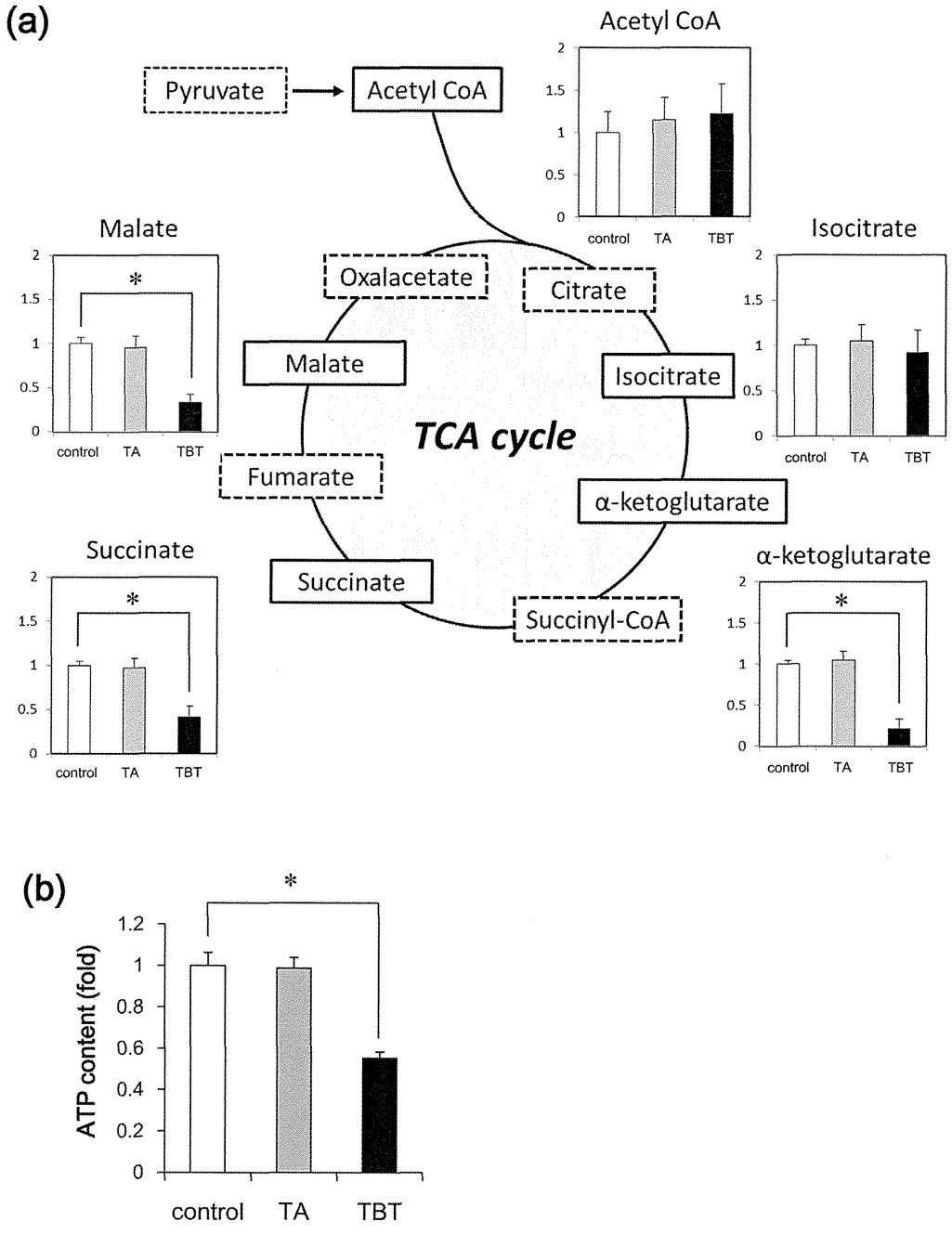

Figure 1 | Metabolomic analysis of NT2/D1 cells exposed to TBT. The cells were exposed to 100 nM TBT or TA for 24 h. (a) The levels of several metabolites, such as acetyl CoA, isocitrate, α-ketoglutarate, succinate and malate, were determined using CE-TOFMS. (b) The intracellular ATP content was determined in the lysed cells. * $P < 0.05$ compared with the corresponding control group.

In the present study, we investigated the molecular target of TBT at nM levels by comprehensive determination of the intracellular metabolites in NT2/D1 cells after TBT exposure. We found that exposure to 100 nM TBT reduced ATP production via NAD-dependent isocitrate dehydrogenase (NAD-IDH) in the cells. This NAD-IDH inhibition resulted in the reduction of the TCA cycle metabolites. In addition, TBT caused neural differentiation through an NAD-IDH-dependent mechanism. We report here that our metabolomic analysis revealed that NAD-IDH is a novel target of TBT in embryonic carcinoma cells.

Results

Metabolomic analysis of NT2/D1 cells exposed to TBT at nM levels. To investigate the non-genomic effects of a well-known endocrine disruptor TBT in human NT2/D1 embryonic carcinoma cells, we comprehensively determined intracellular metabolites using LC/MS. We found that exposure to 100 nM TBT reduced the amounts of TCA cycle components, such as α-ketoglutarate, succinate and malate (Figure 1a). The amounts of acetyl CoA and isocitrate were not changed. We also found that treatment with 100 nM TBT reduced the ATP content of the cells (Figure 1b). In contrast to TBT, exposure to the less toxic tin acetate (TA) did not affect the amount of each metabolite. These data suggest that TBT exposure decreases the amounts of TCA cycle metabolites, resulting in a reduction of ATP content.

NAD-IDH enzyme activity of NT2/D1 cells exposed to TBT at nM levels. Based on the results of the metabolomic analysis, we focused

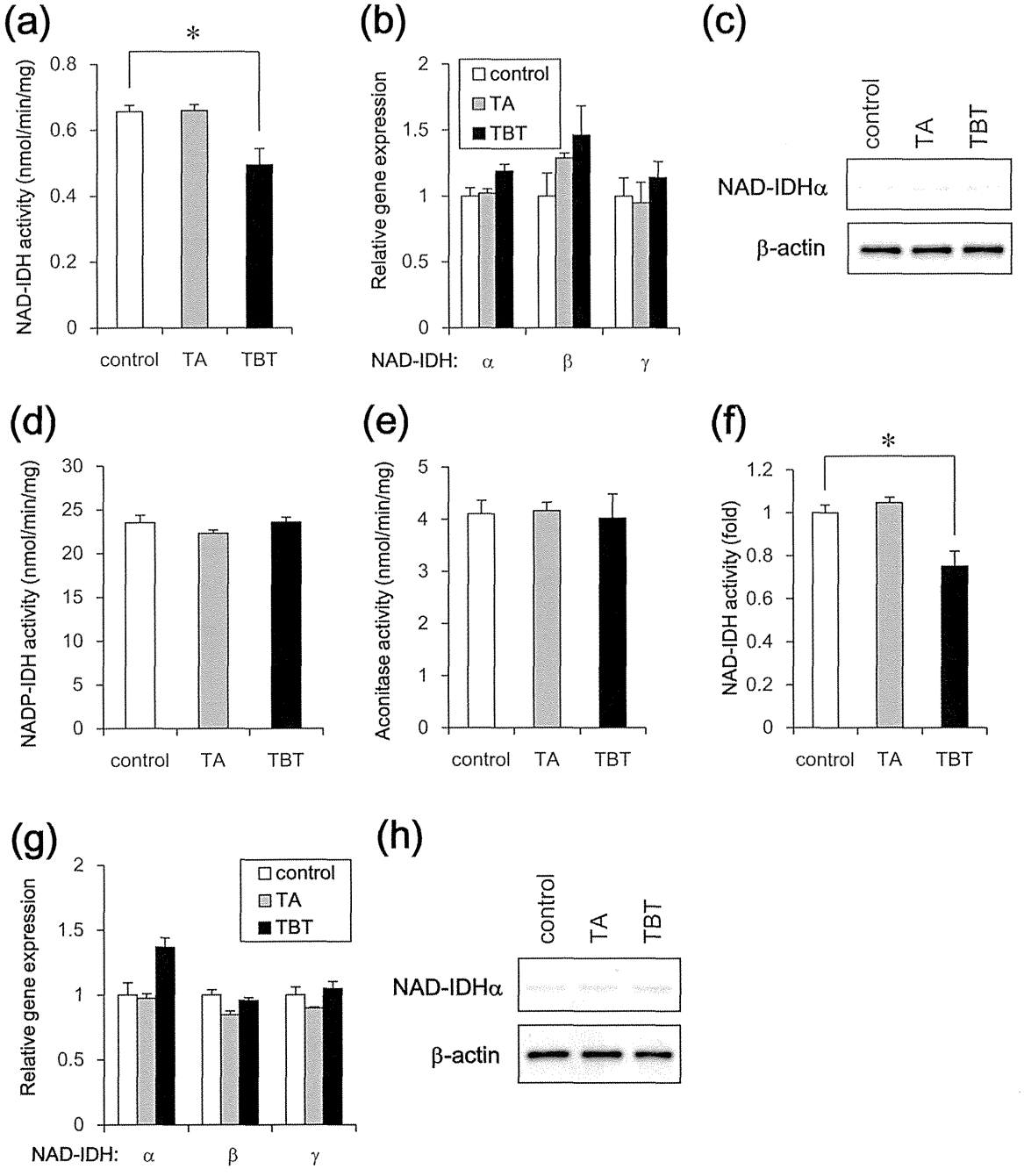

Figure 2 | Effect of TBT exposure on NAD-IDH enzyme activity in NT2/D1 cells. The cells were exposed to 100 nM TBT or TA for 24 h. (a) NAD-IDH activity was determined in the lysed cells. (b) The relative expressions of NAD-IDHα, β, and γ were measured using real-time PCR. The relative changes were normalized to the levels of RPL13. (c) The expression of NAD-IDHα protein was examined by western blot analysis using the anti-NAD-IDHα and anti-β-actin antibodies. Cropped blots were shown and the full-length blots were indicated in Supplementary Fig. 4. (d) NADP-IDH activity was determined in the lysed cells. (e) Aconitase activity was determined in the lysed cells. (f) To induce neuronal differentiation, the NT2/D1 cells were treated with 10 μM retinoic acid (RA) for 14 days. After exposure to 100 nM TBT for 24 h, NAD-IDH activity was determined in the lysed cells. (g) The relative expression levels of NAD-IDHα, β, and γ in the differentiated cells were measured using real-time PCR. The relative changes were normalized to the levels of RPL13. (h) The expression of NAD-IDHα protein was examined by western blot analysis using the anti-NAD-IDHα and anti-β-actin antibodies. Cropped blots were shown and the full-length blots were indicated in Supplementary Fig. 4. * $P < 0.05$ compared with the corresponding control group.

on isocitrate dehydrogenase, which catalyzes the conversion of isocitrate to α-ketoglutarate in the TCA cycle. Eukaryotes have different types of isocitrate dehydrogenases, such as NAD-dependent form (NAD-IDH; EC 1.1.1.41) and NADP-dependent form (NADP-IDH; EC 1.1.1.42)[21]. NAD-IDH is first rate-limiting enzyme in the TCA cycle and catalyzes an irreversible reaction, while NADP-IDH is involved in reversible reaction for biosynthesis via production of NADPH. As shown in Figure 2a, NAD-IDH activity was significantly reduced following TBT treatment. Since NAD-IDH is a heterotetramer composed of two α subunits (catalytic subunit), one β subunit and one γ subunit (regulatory subunit), we examined the expression of each subunit gene. Real-time PCR analysis showed

that the expression of the NAD-IDHα, β and γ genes was not significantly changed by TBT exposure (Figure 2b). The protein expression of catalytic α subunits was not also changed by TBT exposure (Figure 2c). TA exposure did not affect either the enzyme activity or the NAD-IDH expression. We next examined the effect of TBT on NADP-IDH. The activity of NADP-IDH was not affected by TBT exposure (Figure 2d). We further examined the activity of aconitase (EC 4.2.1.3.), which catalyzes the conversion of citrate to isocitrate in the TCA cycle. Aconitase activity was also not affected by TBT exposure (Figure 2e). Thus, these data suggest that the inhibitory effect of TBT is specific to NAD-IDH in the TCA cycle.

To investigate whether TBT cytotoxicity was caused by a genomic transcriptional regulation, we tested the effects of the protein synthesis inhibitor cycloheximide in NT2/D1 cells. Treatment with cycloheximide did not alter the inhibitory effects of TBT on NAD-IDH activity (Figure S1a) and intracellular ATP production (Figure S2a). Moreover, the PPARγ agonist rosiglitazone did not reduce NAD-IDH activity (Figure S1b) and ATP content (Figure S2b). These results suggest that transcriptional regulation is not involved in the inhibition of NAD-IDH activity by TBT.

To examine whether the effect of TBT was selective for embryonic cells, we used NT2/D1 cells that had differentiated in response to retinoic acid. We observed that TBT also inhibited NAD-IDH activity in the differentiated NT2/D1 cells (Figure 2f). Real-time PCR analysis showed that the expression of the NAD-IDHα, β, and γ genes was not significantly affected by TBT exposure (Figure 2g). The protein expression of catalytic α subunits was not also changed by TBT exposure (Figure 2h). TA exposure did not affect either the activity or the NAD-IDH expression. These data suggest that TBT reduces NAD-IDH enzyme activity regardless of the developmental stage of the embryonic carcinoma cells.

Neuronal differentiation of RA-treated NT2/D1 cells exposed to TBT at nM levels. It has been reported that ATP content decreases during the differentiation of human embryonic stem cells into neural stem cells (NSCs)[22]. Therefore, the reduction of ATP caused by TBT treatment might be involved in neuronal differentiation. Moreover, TBT has been reported to cause cell growth arrest in NT2/D1 cells[20]. Because cell growth is generally reduced during differentiation, we examined whether TBT affects the neuronal differentiation process in NT2/D1 cells. Real-time PCR analysis revealed that retinoic acid (RA)-treated NT2/D1 cells showed increased expression of the differentiation markers NeuroD and Math1, confirming that neural differentiation had occurred (Figure 3a). Furthermore, we observed that TBT exposure enhanced the expression levels of these neuronal differentiation markers. Treatment with rosiglitazone had little effect on their expression (Figure S3), suggesting that PPARγ is not involved in neuronal differentiation. Taken together, these data suggest that TBT promotes neuronal differentiation.

Effect of NAD-IDH knockdown on neuronal differentiation in RA-treated NT2/D1 cells. To further investigate whether the neuronal differentiation triggered by TBT exposure is through an NAD-IDH-dependent mechanism, we performed knockdown (KD) of NAD-IDHα, the catalytic subunit of NAD-IDH, using lentivirus-delivered shRNAs. Real-time PCR analysis showed that KD efficiency was approximately 40% (Figure 3b). Due to the partial KD of the NAD-IDHα gene, NAD-IDH activity decreased to a level (22%) comparable to its level following TBT inhibition (24%) (Figure 3c). Further reduction of NAD-IDH activity was not significantly observed after TBT exposure in the NAD-IDHα KD cells. Similar to the effect of TBT, NAD-IDHα KD also reduced the ATP content of the cells (Figure 3d), and caused cell growth inhibition (Figure 3e). Further inhibition of ATP content and cell growth was not significantly observed after TBT exposure in the NAD-IDHα KD cells, suggesting that the NAD-IDH is a possible target of TBT. In addition, we found that NAD-IDHα KD significantly upregulated the expression of the neuronal differentiation markers NeuroD and Math1 (Figure 3f). These data suggest that NAD-IDH mediates TBT-induced neuronal differentiation in embryonic NT2/D1 cells.

NAD-IDH enzyme activity in the brain of rats orally exposed to TBT at low doses. To examine whether the in vitro inhibitory effect of TBT on NAD-IDH is also observed in vivo, adult rats were orally exposed to TBT at doses of 5 and 50 mg/kg. NAD-IDH activity in the cerebral cortex was significantly reduced following exposure to both doses of TBT (Figure 4a). Real-time PCR analysis showed that the expression of the NAD-IDHα, β, and γ genes was not significantly affected by TBT (Figure 4b). The protein expression of catalytic α subunits was not also affected by TBT (Figure 4c). NADP-IDH and aconitase activities were not affected by exposure to either dose of TBT (Figure 4d and e). These data suggest that TBT inhibits NAD-IDH activity both in vitro and in vivo.

Reduction of recombinant hNAD-IDH enzyme activity in E. coli lysate treated with TBT at nM levels. To investigate the mechanism by which TBT inhibits NAD-IDH activity, we examined whether TBT possibly interacts with NAD-IDH or not. Since NAD-IDHα subunit alone has been reported to show no detectable IDH activity, we used an Escherichia coli co-expression system of recombinant human (h) NAD-IDHα,β,γ subunits[23]. As shown in Figure 5a, we confirmed the expression of α subunit of hNAD-IDH protein in the extracts of E. coli transformants using western blot analysis. To check the activity of the recombinant hNAD-IDH, we used irreversible and allosteric NAD-IDH regulators. ADP has been reported to activate NAD-IDH allosterically by lowering the Km for the substrate isocitrate[24]. As expected, ADP increased the activity of hNAD-IDH in our assay system. Conversely, Zn^{2+} has been reported to inhibit several metabolic enzymes, including NAD-IDH, in hepatocytes[25]. We confirmed that Zn^{2+} reduces hNAD-IDH activity. Then, we examined whether TBT directly inhibits hNAD-IDH activity by adding TBT to the E. coli extracts containing hNAD-IDH. Treatment with 100 nM TBT for 1 h significantly reduced the hNAD-IDH activity (Figure 5b). Treatment with TA had little effect. Taken together, these data suggest that TBT inhibits hNAD-IDH activity through its possible interaction, but again we can not be sure that it is through direct binding with the data we have.

***In silico* docking simulation analysis.** To further consider this possible interaction between TBT and hNAD-IDH, we estimate TBT accessibility into hNAD-IDH (EC 1.1.1.41) α and hNADP-IDH (EC 1.1.1.42) homodimers by homology modeling and docking studies. We show the overlaid structure of the calculated hNAD-IDHα and hNADP-IDH (Figure 6a). The ligand binding pocket of hNAD-IDHα was larger than that of hNADP-IDH (Figure 6b). In our docking simulation, TBT was able to access the hNAD-IDHα ligand-binding pocket, whereas the hNADP-IDH pocket was not spacious enough to accommodate TBT (Figure 6c and d). Thus, these studies suggest that the selective inhibition of NAD-IDH by TBT may be due to differences in the pocket volumes between hNAD-IDHα and hNADP-IDH.

Discussion

In the present study, we demonstrate that NAD-IDH is a novel non-genomic target of TBT at nM levels both in vitro and in vivo. We showed that exposure to nM concentrations of TBT reduced the activity of NAD-IDH due to its possible interaction. We also found that TBT exposure caused both inhibition of cell growth and enhancement of neuronal differentiation through its inhibitory effect of NAD-IDH.

Our data suggest that NAD-IDH is a novel target molecule of TBT action. NAD-IDH is a NAD-dependent form of IDH found in NT2/D1 cells and the rat brain (Figure 2–4). Because NAD-IDH is ubi-

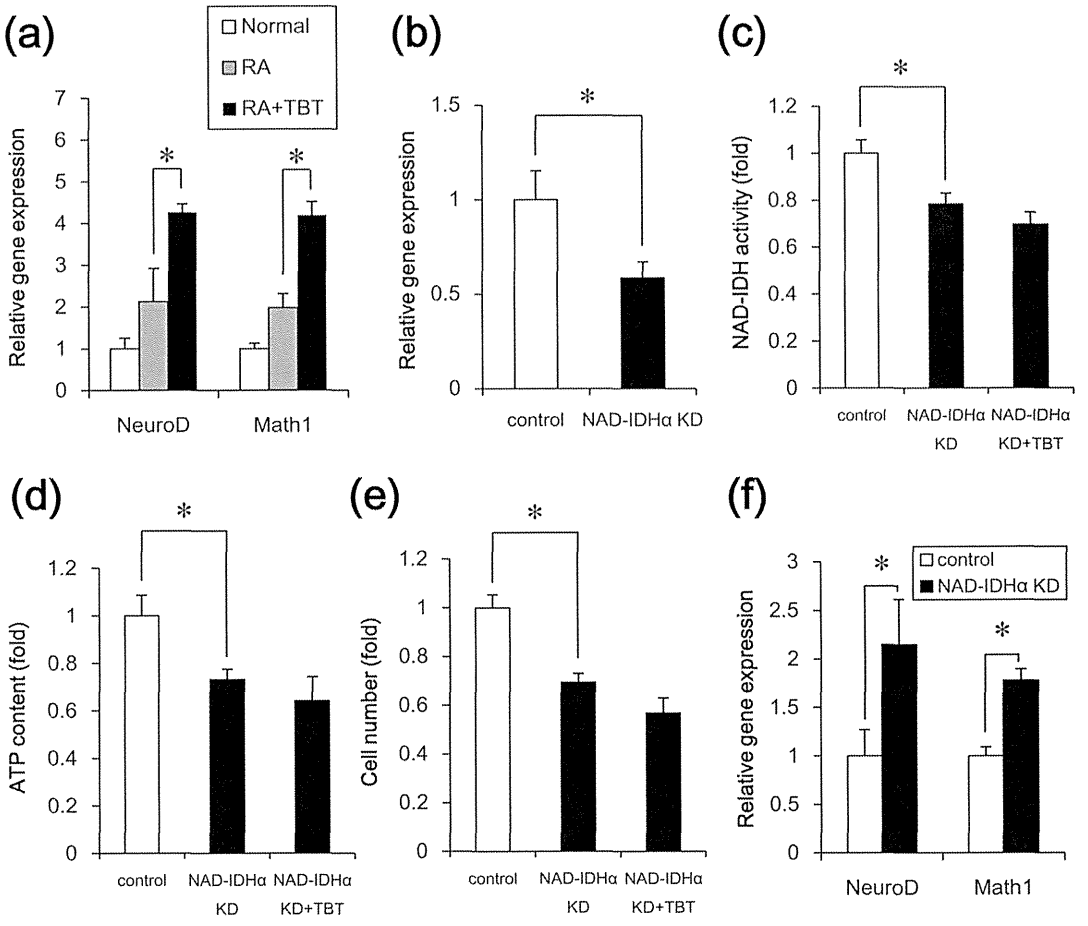

Figure 3 | Effect of TBT exposure or NAD-IDH knockdown on neuronal differentiation in RA-treated NT2/D1 cells. (a) After treatment with RA for 7 days, the cells were treated with RA in the presence of 100 nM TBT for an additional 7 days. The relative expression levels of the neuronal markers NeuroD and Math1 were measured using real-time PCR. The relative changes were determined following normalization to the levels of RPL13. (b–e) The cells were infected with lentiviruses containing a vector encoding a shRNA directed against NAD-IDHα or a scrambled sequence shRNA (control). The infected cells were subjected to selection with 0.5 μg/ml puromycin for 72 h and were then exposed to TBT at 100 nM for 24 h. (b) The relative expression of NAD-IDHα was measured using real-time PCR. The relative change in expression was normalized to the levels of RPL13. (c) NAD-IDH activity was determined in the lysed cells. (d) The intracellular ATP content was determined in the lysed cells. (e) Infected cells were seeded into 100 mm dishes and cultured for 24 h. Cell count was determined using a hemocytometer. (f) After treatment with RA for 7 days, followed by treatment with RA and the shRNA-containing lentiviruses for an additional 7 days, the relative expression levels of the neuronal markers NeuroD and Math1 were measured using real-time PCR. The relative changes were determined following normalization to the levels of RPL13. * $P < 0.05$ compared with the corresponding group.

quitously expressed, the toxicity of TBT might be observed in various cell types. Several TCA cycle enzymes have been reported to contribute to cell proliferation. For example, NADP-IDH plays a role for cell growth under hypoxic conditions in human glioblastoma cells[26]. Another study has shown that aconitase mediated cell proliferation via ATP production in human prostate carcinoma cells[27]. NAD-IDH has been shown to regulate the metabolic fluxes and the generation of ATP in the TCA cycle[28]. Therefore, it is likely that NAD-IDH is a target of TBT cytotoxicity and regulates cell growth in embryonic carcinoma cells.

In addition to cell growth inhibition, we also showed that neural differentiation is enhanced by TBT exposure or NAD-IDH inhibition (Figure 3). Consistent with our data, overexpression of NAD-IDHα has been shown to reduce neuronal differentiation and neurite outgrowth through the inactivation of MAPK phosphorylation in PC12 cells[29]. Because TBT exposure has been reported to induce neurotoxicity via ERK and p38MAPK phosphorylation in cultured rat cortical neurons[30], TBT exposure might cause cytotoxicity through the MAPK pathways. Thus, a non-genomic pathway plays a role in TBT toxicity. Indeed, the genomic target PPARγ and treatment with cycloheximide did not alter the effects of TBT (Figure S1–3). It is unlikely that transcriptional regulation is involved in NAD-IDH activity and the enhancement of neuronal differentiation. The downstream pathway of TBT-NAD-IDH should be determined in embryonic carcinoma cells.

Our data suggest that TBT regulates NAD-IDH activity through possible interaction. However, we can not conclude that it is through direct binding. Previous reports have suggested that TBT can bind to multiple target proteins, such as PPARγ, RXR, F1F0 ATP synthase and 11β-hydroxysteroid dehydrogenase (11β-HSD) type 2, with broad specificity[19,31]. For example, TBT binds the RXRα ligand-binding domain through a covalent bond between the tin atom and the Cys residue[32]. TBT also binds 11β-HSD type 2 by interacting with several Cys residues in the active site[31]. Because the ligand-binding pocket of hNAD-IDHα contains several Cys residues[33] and has enough space to accommodate TBT, TBT might bind to hNAD-IDHα via Cys residues. Future conformational analysis, including X-ray crystallography or computer simulation, and mutagenesis studies should be performed to determine whether TBT binds to hNAD-IDHα or not.

Our metabolomic analysis showed that TBT inhibited cell growth and enhanced neuronal differentiation through possible direct

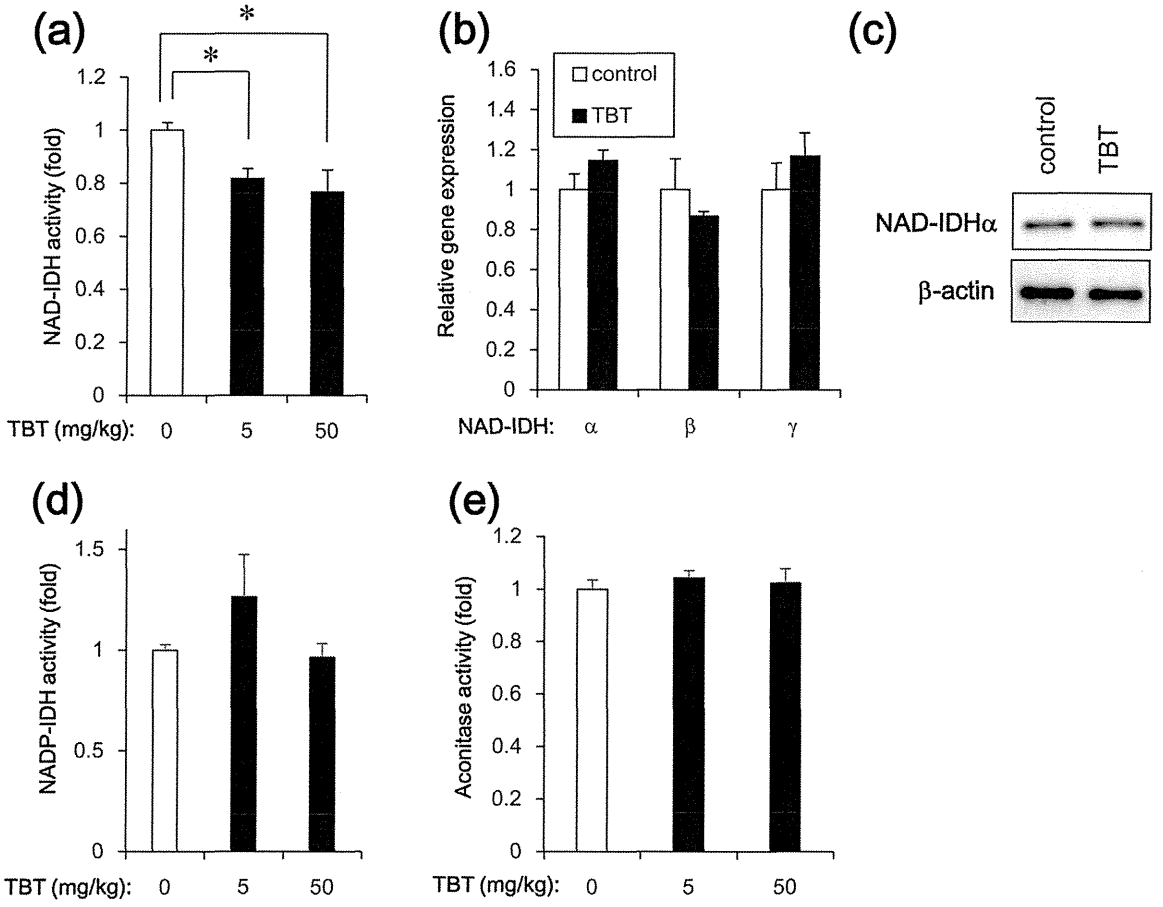

Figure 4 | NAD-IDH enzyme activity in the brain of rats orally exposed to TBT at doses of 5 and 50 mg/kg for 6 h. (a) NAD-IDH activity was determined in the brain lysates. (b) The relative expression levels of NAD-IDHα, β, and γ in rats exposed to 50 mg/kg TBT were measured using real-time PCR. The relative changes were normalized to the levels of RPL13. (c) The expression of NAD-IDHα protein was examined by western blot analysis using the anti-NAD-IDHα and anti-β-actin antibodies. Cropped blots were shown and the full-length blots were indicated in Supplementary Fig. 4. (d) NADP-IDH activity was determined in the brain lysates. (e) Aconitase activity was determined in the brain lysates. * $P < 0.05$ compared with the corresponding TBT 0 group.

inhibition of NAD-IDH activity in human embryonic carcinoma cells. Thus, comprehensive approach of non-genomic metabolic pathway might be a powerful tool to elucidate the mechanism of EDC action.

Methods

Chemicals and reagents. TBT was obtained from Tokyo Chemical Industry (Tokyo, Japan). Tin acetate (TA) and rosiglitazone were obtained from Sigma-Aldrich (St. Louis, MO, USA). All other reagents were of analytical grade and were obtained from commercial sources.

Cell culture. NT2/D1 cells were obtained from the American Type Culture Collection. The cells were cultured in Dulbecco's modified Eagle's medium (DMEM; Sigma-Aldrich) supplemented with 10% fetal bovine serum (FBS; Biological Industries, Ashrat, Israel) and 0.05 mg/ml penicillin-streptomycin mixture (Life Technologies, Carlsbad, CA, USA) at 37°C and 5% CO2. For neural differentiation, all-trans retinoic acid (RA; Sigma-Aldrich) was added to the medium twice a week at a final concentration of 10 μM.

Determination of TCA cycle metabolites. Intracellular metabolites were extracted and used for subsequent capillary electrophoresis time-of-flight mass spectrometry (CE-TOFMS) analysis, as previously described. The amounts of the metabolites were determined using an Agilent CE capillary electrophoresis system (Agilent Technologies, Waldbronn, Germany) equipped with an Agilent G3250AA LC/MSD TOF system (Agilent Technologies, Palo Alto, CA), an Agilent 1100 series isocratic HPLC pump, a G1603A Agilent CE-MS adapter kit, and a G1607A Agilent CE-electrospray ionization 53-MS sprayer kit. For system control and data acquisition, the G2201AA Agilent ChemStation software was used for CE, and the Agilent TOF (Analyst QS) software was used for the TOFMS.

Measurement of intracellular ATP levels. The intracellular ATP content was measured using the ATP Determination Kit (Life Technologies), according to the manufacturer's protocol. Briefly, the cells were washed and lysed with 0.1% Triton X-100/PBS. The resulting cell lysates were added to a reaction mixture containing 0.5 mM D-luciferin, 1 mM DTT, and 1.25 μg/ml luciferase and incubated for 30 min at room temperature. Luminescence was measured using a Wallac1420ARVO fluoroscan (Perkin-Elmer, Waltham, MA, USA). The luminescence intensities were normalized to the total protein content.

Isocitrate dehydrogenase (IDH) activity assay. IDH activity was determined using the commercial Isocitrate Dehydrogenase Activity Colorimetric Assay Kit (Biovision, Mountain View, CA, USA), according to the manufacturer's instructions. Briefly, NT2/D1 cells were lysed in an assay buffer provided in the kit. The lysate was centrifuged at 14,000 g for 15 min, and the cleared supernatant was used for the assay. NADP or NAD was used as the substrate for the NADP-IDH or NAD-IDH assay, respectively.

Real-time PCR. Total RNA was isolated from NT2/D1 cells using the TRIzol reagent (Life Technologies), and quantitative real-time reverse transcription (RT)-PCR with the QuantiTect SYBR Green RT-PCR Kit (QIAGEN, Valencia, CA, USA) was performed using an ABI PRISM 7900HT sequence detection system (Applied Biosystems, Foster City, CA, USA), as previously reported. The relative changes in the transcript amounts of each sample were normalized to the mRNA levels of ribosomal protein L13 (RPL13). The following primer sequences were used for real-time PCR analysis: human NAD-IDHα: forward, 5′-ATCGGAGGTCTCGGTGTG-3′, reverse, 5′-AGGAGGGCTGTGGGATTC-3′; human NAD-IDHβ: forward, 5′-GCCTC-AGCCGCATATCATAG-3′, reverse, 5′-GAGCAGGTGCTGAGTTCCAT-3′; human NAD-IDHγ: forward, 5′-TTAGCGGACGGAGGAATTGT-3′, reverse, 5′-CAGCCCTTCTCTGCCGT-3′; human NeuroD: forward, 5′-GGAAACGA-ACCCACTGTGCT-3′, reverse, 5′-GCCACACCAAATTCGTGGTG-3′; human Math1: forward, 5′-GTCCGAGCTGCTACAAACG-3′, reverse, 5′-GTGGTGGT-GGTCGCTTTT-3′; human RPL13: forward, 5′-CATCGTGGCTAAACAGGTAC-

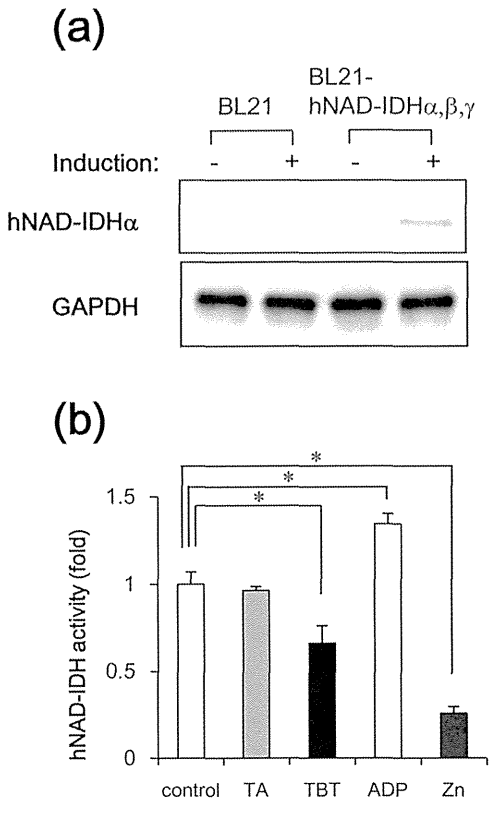

Figure 5 | Reduction of NAD-IDH enzyme activity by interaction with TBT in an E. coli expression system. (a) After the expression of pHIDHα, β, γ was induced by culturing E. coli BL21 transformants at 25°C for 20 h, crude extracts were prepared and were subjected to western blot analysis using the anti-NAD-IDHα and anti-GAPDH antibodies. Cropped blots were shown and the full-length blots were indicated in Supplementary Fig. 4. (b) After treatment with 100 nM TBT for 1 h, NAD-IDH activity was determined in the crude extracts. ADP (100 μM) and Zn^{2+} (2 mM) were used as positive and negative controls, respectively. * $P < 0.05$ compared with the corresponding control group.

TG-3′, reverse, 5′-GCACGACCTTGAGGGCAGCC-3′; rat NAD-IDHα: forward, 5′-TGGGTGTCCAAGGTCTCTC-3′, reverse, 5′-CTCCCACTGAATAGGTG-CTTTG-3′; rat NAD-IDHβ: forward, 5′-AGGCACAAGATGTGAGGGTG-3′, reverse, 5′-CAGCAGCCTTGAACACTTCC-3′; rat NAD-IDHγ: forward, 5′-TGGGCGGCATACAGTGACTA-3′, reverse, 5′-TTGGAGCTTACATGCAC-CTCT-3′; rat RPL13: forward, 5′-GGCTGAAGCCTACCAGAAAG-3′, reverse, 5′-CTTTGCCTTTTCCTTCCGTT-3′.

Aconitase activity assay. Aconitase activity was determined using the commercial Aconitase Activity Colorimetric Assay Kit (Biovision), according to the manufacturer's instructions. Briefly, NT2 cells were lysed in an assay buffer provided in the kit. The lysate was centrifuged at 14,000 g for 15 min, and the cleared supernatant was used for the aconitase assay.

NAD-IDHα knockdown experiment. Transient gene knockdown was performed using NAD-IDHα shRNA lentiviruses from Sigma-Aldrich (MISSION® shRNA) according to manufacturer's protocol. A scrambled hairpin sequence was used as a negative control. Briefly, the cells were infected with the viruses at a multiplicity of infection of 10, in the presence of 8 μg/ml hexadimethrine bromide (Sigma-Aldrich), for 24 h, and were then subjected to selection with 0.5 μg/ml puromycin for 72 h prior to functional analyses.

Tissue preparation. The present study was approved by the animal ethics committee and was conducted in accordance with the regulations on the use of living modified organisms of Hiroshima University. Male Slc:Wistar/ST rats (8 weeks old) were purchased from Japan SLC, Inc. (Shizuoka, Japan). They were housed under controlled temperature, 12 h light/dark cycle, and humidity (75 ± 5%) for at least 1 week prior to experiments. Standard pellet food and water were provided ad libitum. TBT solution (5 and 50 mg/kg body weight) was orally administered to rats. TBT was dissolved in polyethylene glycol. The whole brain was exposed by the use of fine scissors and forceps, and the frontal part of cerebral cortex was excised from the brain.

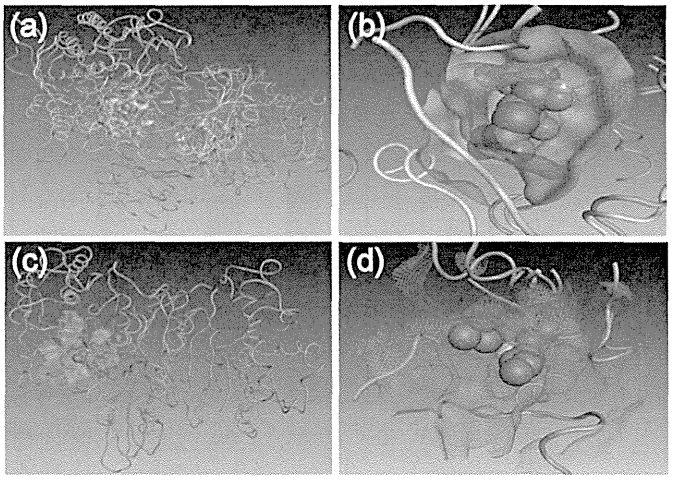

Figure 6 | In silico docking simulation analysis. (a) Overlaid structures of the calculated hNAD-IDHα (orange) and hNADP-IDH (cyan) homodimers bound to isocitric acid (Space-filling model). (b) The ligand binding pockets of the hNAD-IDHα (solid) and hNADP-IDH (wireframe) proteins. (c, d) Docking structure of hNAD-IDHα containing TBT (Space-filling model).

Transformation and Expression of Recombinant Human NAD-IDH Proteins in E. coli. pHIDHαβ1γ plasmid DNA (a kind gift from Dr. T. L. Huh) was used to transform E. coli BL21 (DE3) ultracompetent cells (BioDynamics, Tokyo, Japan). The colonies with positive inserts were subcultured and grown overnight at 37°C in LB medium (2 ml) supplemented with ampicillin (0.1 mg/ml). To express the enzyme, 15 ml tubes containing 2 ml of LB medium with 0.1 mg/ml ampicillin were inoculated with freshly grown E. coli cells (1% v/v), and these cultures were grown at 37°C while being shaken at 220 rpm for 4 h. The flasks were then temporarily placed in chilled water to lower the culture temperature to 25°C. Protein expression was induced in the cells by shaking at a lower speed of 140 rpm with minimal aeration at 25°C for 20 h. Then, 2 ml of the cell culture was centrifuged at 6,000 g for 15 min to separate the cells from the media, and the pellet was suspended in a total volume of 300 μl of cold assay buffer, a component of Isocitrate Dehydrogenase Activity Assay Kit. The suspended cells were subjected to 3 cycles of freeze-thaw before sonication (5 cycles of 15 sec sonication and 45 sec rest) and lysed. The cell lysate was centrifuged at 14,000 g for 15 min, and the cleared supernatant (crude extract) was separated. Recombinant human NAD-IDH activity was determined by subtracting basal activity in the crude extract from control BL21 cells.

Western blot analysis. Western blot analysis was performed as previously reported[34]. Briefly, the cells were lysed with Cell Lysis Buffer (Cell Signaling Technology, Danvers, MA, USA), and the proteins were separated by sodium dodecyl sulfate (SDS)-polyacrylamide gel electrophoresis and electrophoretically transferred to Immobilon-P (Millipore, Billerica, MA, USA). The membranes were probed with an anti-NAD-IDH (IDH3) α polyclonal antibody (1 : 1,000; Abcam, Cambridge, UK), an anti-β-actin monoclonal antibody (1 : 5,000; Sigma-Aldrich), and an anti-GAPDH monoclonal antibody (1 : 2,000; Abcam). The membranes were then incubated with secondary antibodies against rabbit or mouse IgG conjugated to horseradish peroxidase (Cell Signaling Technology). The bands were visualized using the ECL Western Blotting Analysis System (GE Healthcare, Buckinghamshire, UK), and the images were acquired using a LAS-3000 Imager (FUJIFILM UK Ltd., Systems, Bedford, UK). The density of each band was quantified using the ImageJ software (NIH, Bethesda, MD, USA).

In silico docking simulation studies. Homology modeling and docking studies of the human NAD-IDHα (hNAD-IDHα) and NADP-IDH (hNADP-IDH) homodimers were performed using Molecular Operating Environment (MOE) 2012.10. The models of hNAD-IDHα and hNADP-IDH were constructed based on the crystallographic structure of the porcine NADP-IDH homodimer (PDB: 1LWD)[35] using the standard protocols in MOE 2012.10. The docking simulations of the TBT-bound hNAD-IDHα and hNADP-IDH were carried out using ASEDock[36]. The TBT ligand was assigned in ASEDock, and the conformations were calculated using MMFF94S force field[37].

Statistical analysis. Results are shown as mean ± S.D. Statistical analysis was performed using one-way ANOVA followed by Dunnett's test. Differences at $P < 0.05$ were considered to be significant.

1. Toppari, J. *et al.* Male reproductive health and environmental xenooestrogens. *Environ. Health Perspect.* **104**, 741–803 (1996).